2024

Characterization of a novel bioluminescent reporter protein for the non-invasive preclinical imaging of viral infection

BOSTON UNIVERSITY

ARAM V. CHOBANIAN & EDWARD AVEDISIAN SCHOOL OF MEDICINE

Thesis

CHARACTERIZATION OF A NOVEL BIOLUMINESCENT REPORTER PROTEIN FOR THE NON-INVASIVE PRECLINICAL IMAGING OF VIRAL INFECTION

by

NADER CHEHADEH

A.A., North Shore Community College, 2018
B.S., University of Massachusetts, Boston, 2020

Submitted in partial fulfillment of the

requirements for the degree of

Master of Science

2024

Approved by

First Reader

Elizabeth Duffy, M.A.
Assistant Professor of Pathology & Laboratory Medicine

Second Reader

Florian Douam, Ph.D.
Assistant Professor of Virology, Immunology & Microbiology

DEDICATION

I dedicate this paper to *Heterocarpus ensifer*.

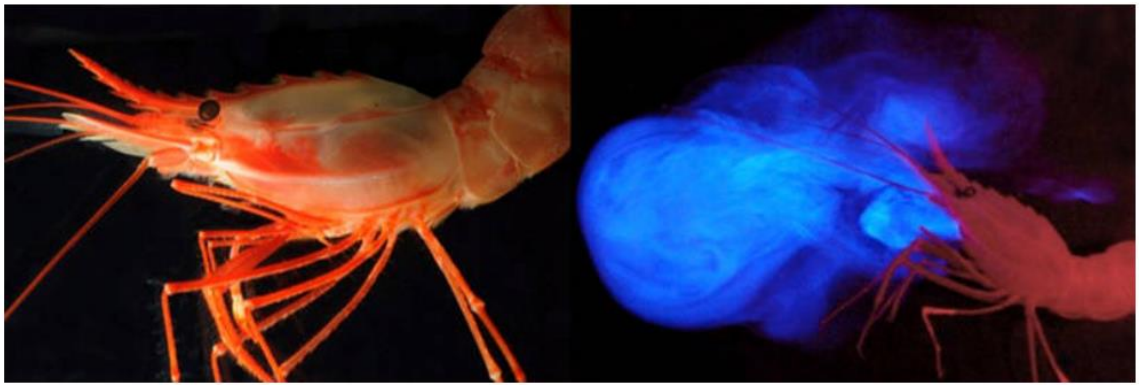

Credit to Sönke Johnsen and Katie Thomas.

ACKNOWLEDGMENTS

I'd like to thank the entirety of the Douam Lab for welcoming me into their space for the past year and a half with open arms. Who I've become as a technician and researcher has been shaped and molded by the insights and wisdom of every member.

CHARACTERIZATION OF A NOVEL BIOLUMINESCENT REPORTER PROTEIN FOR THE NON-INVASIVE PRECLINICAL IMAGING OF VIRAL INFECTION

NADER CHEHADEH

ABSTRACT

RNA viruses pose significant public health concerns due to their high mutation rates. This ability enables the rapid evolution of endemic viruses and the emergence of new strains with enhanced virulence. Many RNA viruses originate from animals, facilitating zoonotic transmission and the potential for pandemics. RNA viruses exhibit a wide range of hosts, leading to interspecies transmission and the emergence of novel diseases. Treatment options are often limited, and vaccine development can be challenging due to genetic variability [1,2].

An exception that's overcome this challenge is the Yellow Fever Virus (YFV). In the early 20th century, a live attenuated strain of the YFV (17D) was deemed as an effective vaccine against the mosquito-borne virus. Despite this progress, the virus persists in endemic regions of Africa and South America, necessitating ongoing study and surveillance. Continued research into the virus's biology, epidemiology, and transmission dynamics is essential for maintaining global health security against this enduring threat [3,4].

The integration of bioluminescent reporter genes into viral genomes presents a cutting-edge approach in understanding how a virus propagates throughout the host. This

allows for researchers to non-invasively track the infection's progression from start to finish in laboratory animal models [5]. The aim of this study is to characterize a novel bioluminescent reporter protein with increased tissue penetration ability for the comprehensive non-invasive preclinical imaging of YFV infection. Such tool could open novel avenues for the identification of critical host and viral determinants of viral disease, and the evaluation of antiviral countermeasures.

In-vitro characterization of the novel reporter, NanoLSS1, was first achieved by transducing A549 (Adenocarcinoma Human Alveolar Basal Epithelial) cells using a lentiviral transduction system to demonstrate how the reporter emits signal at different wavelengths [6]. Using a Bioluminescent Resonance Energy Transfer (BRET) system, the reporter exhibits both excitation and emission peaks, with the excitation peak at 460nm and an emission peak of 615nm [7]. Both spectrophotometer and in vivo imaging system (IVIS) platform were used to capture and quantify the emitted signals from the transduced cells lines [8].

Specifically, different conformational variations of the NanoLSS1 were analyzed to determine which exhibited the highest photon intensities emitted at multiple wavelengths. The most optimal variation of the reporter was used in later experiments [11]. By mimicking tissue depth using slices of ham overlayed over the transduced cell lines, we also confirmed that NanoLSS1 had the highest degree of tissue penetrance when emitting signal [10] compared to conventional bioluminescent reporter, such as Nanoluc [11].

Utilizing a reverse genetics recombinant virus system, reporter proteins can be introduced into a viral genome through PCR, resulting in viral particles expressing the desired reporter genes upon infection and viral replication [9]. Using such system, we successfully developed and rescued a NanoLSS1-expressing 17D virus. This newly generated virus can infect 293T (Human Embryonic Kidney) and Huh7.5 (Hepatocyte-Derived Carcinoma) cells, infection is associated with BRET function and a bioluminescence emission peak of 615nm. The recombinant virus system was also implemented to generate YFV-17D expressing Nanoluc to be used as a control for future mouse infection studies.

Collectively, my work successfully characterized a novel bioluminescent reporter protein for investigating viral dissemination into an infected host. My work open avenues for unravelling novel facets of viral pathogenesis and developing innovative antiviral countermeasures.

TABLE OF CONTENTS

LIST OF TABLES

LIST OF FIGURES

LIST OF ABBREVIATIONS

293T ..... Human Embryonic Kidney Cells

A549 ..... Adenocarcinoma Human Alveolar Basal Epithelial Cells

ATP ..... Adenosine 5-triphosphate

BRET ..... Bioluminescent Resonance Energy Transfer

BSL ..... Biosafety Level

cDNA ..... Complementary Deoxyribonucleic Acid

CPER ..... Circular Polymerase Extension Reaction

CPE ..... Cytopathic Effects

DAPI ..... 4’,6-diamidino-2-phenylindole

DMEM ..... Dulbecco's Modified Eagle Medium

FBS ..... Fetal Bovine Serum

Fz ..... Furimazine

GFP ..... Green Fluorescent Protein

Huh7.5 ..... Hepatocyte-Derived Carcinoma Cell Line

IACUC ..... Institutional Animal Care and Use Committees

LSS1b ..... Long Stokes Shift 1b

Nluc ..... Nano-luciferase

Opti-MEM ..... Minimal Essential Medium

P/S ..... Penicillin Streptomycin

PCR ..... Polymerase Chain Reaction

PFA ..... Paraformaldehyde

PFU .....Plaque Forming Unit

TB ..... Terrific Broth

YFV.....Yellow Fever Virus

INTRODUCTION

Yellow Fever Virus: A Forgotten Foe

Belonging to the *Flaviviridae* family of viruses, Yellow Fever Virus (YFV) is an enveloped positive sense, single stranded RNA virus. YFV is endemic to regions in West, Central, and East Africa with recorded outbreaks also documented as well as in Central and South America [4]. Additionally, the ongoing climate change crisis is driving an expansion of endemic regions of YFV and other flaviviruses increasing the threat of Arbovirus outbreaks [12]. The increase in YFV cases in non-endemic or low risk areas has raised the public concern about YFV, however there are still no effective antiviral treatment options for the disease [1].

While the vaccine for YFV (YFV-17D) is one of the most effective vaccines to date, its distribution is challenging due to increased demand in endemic areas and manufacturing constraints from the complexity of producing the live attenuated virus. These compounding issues necessitate the need to enhance our understanding of YFV virus, its transmission, and disease caused by infection [13].

The primary carriers of the virus are the *Aedes* or *Haemagogus* mosquito species. Transmission to humans occurs through from the bite of an infected mosquito, which typically happens when a mosquito feeds on a non-human primate that is carrying YFV and subsequently bites a person. This transmission between a non-human primate, mosquito and human is known as the sylvatic cycle and is the primary cause of YFV spread. Additionally, spread can occur through human-to-mosquito-to-human transmission in urban areas where the sylvatic cycle is not possible. Despite vaccination

efforts and other initiatives such as mosquito eradication there are still outbreaks of YFV in endemic areas [13].

History of YFV

Yellow fever has a long and devastating history marked by several significant outbreaks (Figure 1). The first recorded epidemic occurred in 1648 in the Yucatán Peninsula, though specific details are scarce. One of the most notable early outbreaks was in Philadelphia in 1793, where the disease claimed about 5,000 lives out of a population of 50,000, causing widespread panic and highlighting the limitations of contemporary medical knowledge [14].

In the 20th century, scientific advancements began to change the trajectory of the disease. In 1900, the Yellow Fever Commission confirmed that the *Aedes* aegypti mosquito was the primary vector, leading to better prevention strategies. By 1937, Max Theiler developed the 17D yellow fever vaccine, a critical tool in controlling the disease [13].

Despite these advancements, yellow fever continued to cause significant outbreaks. In 1986, West Africa experienced a severe epidemic with approximately 20,000 cases and 4,000 deaths, prompting international control efforts. Between 2005 and 2008, Sudan faced an epidemic that resulted in 732 cases and 166 deaths [15,16].

The 21st century has seen ongoing challenges with yellow fever. The World Health Organization's (WHO) launch of the Eliminate Yellow fever Epidemics (EYE) strategy in 2013 aimed to significantly reduce yellow fever cases through increased vaccination and surveillance efforts. Advances in molecular biology from the 1960s to

the 1990s also contributed to a better understanding of the virus and improved prevention strategies [17].

In 2016, Angola and the Democratic Republic of Congo reported over 7,000 suspected cases and at least 400 deaths. The following year, Brazil experienced a severe outbreak with 777 confirmed cases and 261 deaths. In 2021, Ghana had 202 suspected cases of Yellow Fever (YF) including 70 confirmed cases and 35 deaths [18].

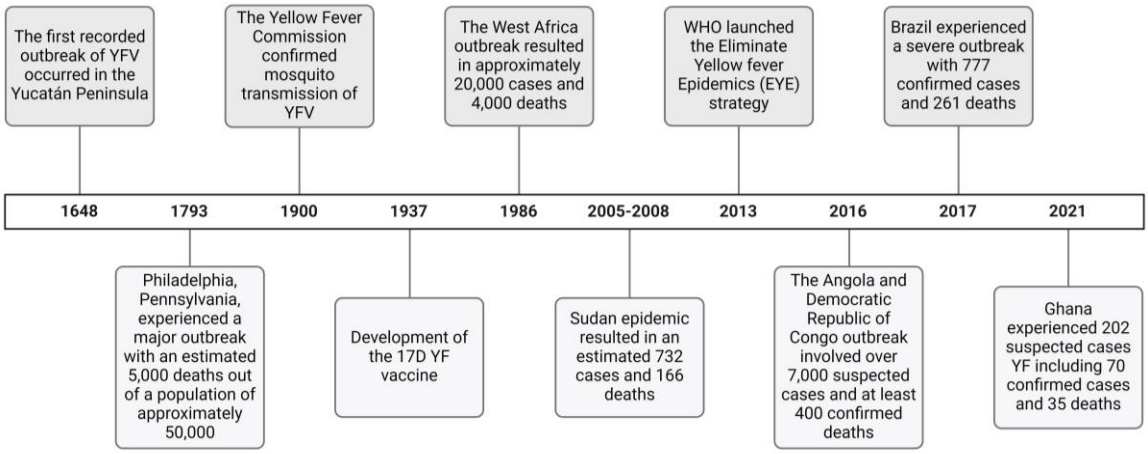

Figure 1: History of Yellow Fever Virus from 1648-2022

Clinical Manifestations of YFV

In many cases of YFV infection, patients are asymptomatic. However, the infection can lead to a wide range of symptoms depending on the progression of the disease. The initial stages involve an incubation period of 3-6 days, typically without any signs of illness. After this period, individuals may experience flu-like symptoms such as fever, headache, vomiting, and loss of appetite [10].

While many symptomatic YFV infections result in improvement and full recovery, some progress to a state of viremia. In this second phase, more severe symptoms begin to develop. The main organs affected are the kidneys and liver, leading to jaundice, renal failure, and significant hepatic dysfunction. The infected individual may also show signs of viral hemorrhagic fever, marked by bleeding from the mouth, nose, and eyes [10,19]

Understanding the progression of YFV infection is crucial. After the initial bite from an infected mosquito, the virus migrates to the lymph nodes and is later carried by dendritic cells. The initial replication phase occurs in the lymph nodes before the virus moves to the liver, where replication intensifies in hepatocytes, causing inflammation [20]. Severe inflammation, known as a cytokine storm, results from a strong proinflammatory response [21,22]. This, in turn, causes vasculitis, a narrowing of the blood vessels due to immune system dysregulation, leading to shock from blood loss. Widespread inflammation triggered by the body's response to YFV infection could potentially lead to multi-organ dysfunction [23].

These combined symptoms contribute to a high mortality rate of 20-50% in untreated cases. This emphasizes the importance of prompt and appropriate treatment for YFV infections to reduce the risk of severe outcomes [24].

Vaccine Origins

In the early 20th century, researchers were able to isolate and study a pathogenic variant of the YFV. Nicknamed "Asibi", after the West African patient it was derived from, it is the parent strain of the vaccine that is commercially available today. The

process of developing the YFV vaccine involved serially passaging the Asibi strain by inoculating the virus in mouse embryonic and brain tissues. The virus was extracted from the tissues and further inoculated. This cycle was repeated several hundred times during which the virus acquired mutations induced by adapting to the mouse host tissues. Researchers monitored and selected for the virus progeny with reduced virulence [4]. The final attenuated strain (17D) was chosen for its ability to stimulate an immune response without causing disease, forming the basis of the YFV vaccine. Since there are no approved antiviral treatments for YFV infection, vaccination is the primary method of infection control [25]. By eliciting a robust immune response, the YFV-17D vaccine provides long-term protection (30-35 years) against pathogenic strains of the virus without causing disease [3]. With infections in the United States considered very rare, visitors entering Yellow Fever endemic regions are recommended to be vaccinated [13].

Differences Between 17D and Asibi

The Asibi and 17D strains of YFV show significant differences that influence their pathogenicity and immunogenicity. Genetically, they differ by 32 amino acids and 68 nucleotides, which play a crucial role in their distinct behaviors [26]. 12 specific amino acid differences in located in the E envelope glycoprotein have been shown to significantly affect the virus's entry pathways and immune response. YFV-17D uses different cell entry pathways and promotes more efficient binding to host cells, resulting in a robust antiviral response [27, 28]. In primary human vascular endothelial cells and immune cells like Kupffer cells, macrophages, and dendritic cells, YFV-Asibi triggers a stronger and more prolonged pro-inflammatory response compared to YFV-17D [29, 30].

Moreover, in dendritic cells, YFV-17D's restricted replication prevents apoptosis, aiding better immune system activation and promoting the production of key cytokines in CD4+ T cells, enhancing adaptive immunity [31]. Understanding these differences between the Asibi and 17D strains is essential for designing better vaccines and therapeutic strategies.

Reactions to Yellow Fever Vaccine

With over 500 million administered doses of the YFV vaccine, it remains one of the most successful and safe vaccines to date [32]. Although rare, there have been documented cases of adverse reactions to the YFV vaccine. Mild reactions include headaches, myalgia, and a low fever which typically subside within a few days of receiving the vaccine. Severe reactions are considered even more rare but are worth noting. They can range from neurological diseases such as meningoencephalitis or anaphylaxis to viscerotropic disease. Recent cases of yellow fever vaccine-associated viscerotropic disease (YEL-AVD) were reported in individuals over the age of 60 in Brazil, and historically, YEL-AVD has been documented with a bad lot of the vaccine in the 1990s [33, 34].

While the overall risk of severe symptoms developing from vaccine administration is low, the vaccine’s benefit to residents in endemic areas should be considered. Travelers should consider being vaccinated when entering endemic areas or if laboratory personnel are routinely working with the wild-type virus. Other factors, such as residents living in high-risk settings where *Aedes* Aegyptus mosquitoes are prominent, should also be considered [35].

Molecular Overview of YFV

YFV is an enveloped virus with a single-stranded, positive-sense RNA genome of about 11,000 nucleotides. This genome contains a single open reading frame encoding a large polyprotein of 3,400 amino acids, which is processed into ten viral proteins: three structural proteins (Core, PrM, and E) and seven non-structural proteins (NS1, NS2A, NS2B, NS3, NS4A, NS4B, and NS5). YFV initially binds non-specifically to glycosaminoglycan heparan sulfate on host cells like hepatocytes and dendritic cells. The exact receptor for the E envelope glycoprotein is unknown [36]. The assembly of YFV particles is not fully understood, but it is thought that newly assembled nucleocapsids, composed of core proteins and viral RNA, are engulfed within endoplasmic reticulum (ER) membranes harboring the envelope glycoproteins E and PrM. These immature particles migrate to the trans-Golgi network where they undergo glycosylation and maturation [37,38,39]. The complete life cycle of YFV, including mechanisms of entry, assembly, and replication, remains incompletely understood, necessitating further research to develop potent antiviral strategies.

Implementation of Reporter Viruses for In-vitro Imaging

Using engineered reporter viruses, the spread of viral infection can be observed in real time. Measurable signals such as fluorescence or bioluminescence are produced by these viruses expressing different reporter genes (Figure 2). Infection dynamics, such as the different stages of viral replication, viral pathogenesis, and susceptibility of certain cell types or tissues, can be monitored using these reporter viruses [14,15].

Reporter viruses can potentially play a crucial role in tracking the effectiveness of antiviral drugs in real time, providing insights into drug mechanisms and potential resistance development. Additionally, they facilitate high-throughput screening assays to pinpoint host factors involved in viral replication, thereby identifying potential targets for therapeutic intervention. [40, 41].

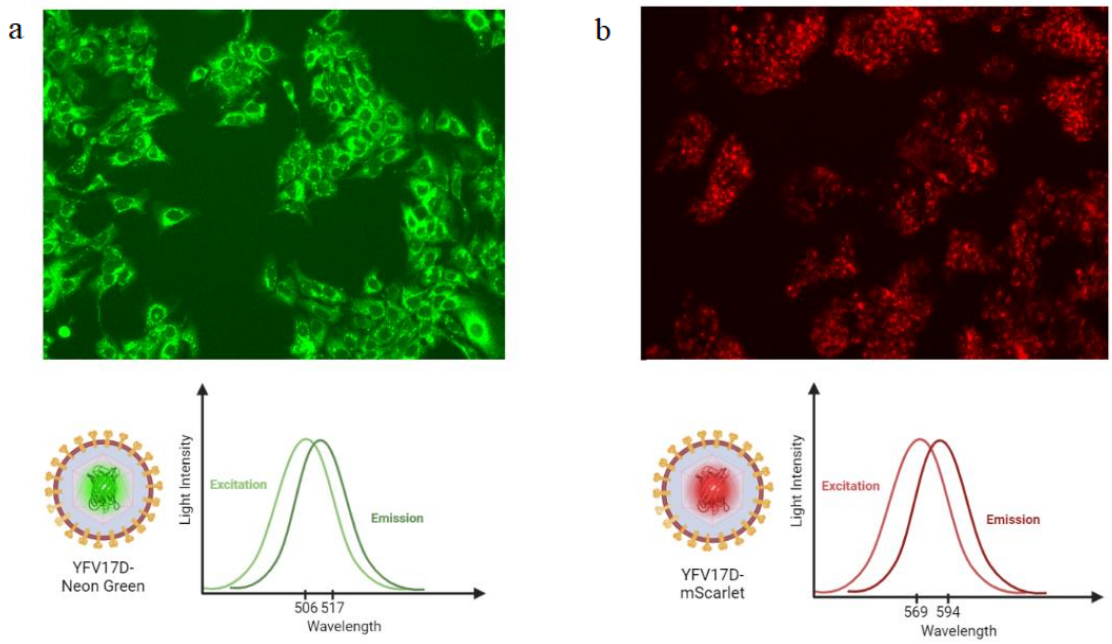

Figure 2: **YFV-17D Reporter Viruses for *in vitro* Imaging** A) Huh7.5 cells infected with YFV-17 expressing the neon green gene and its corresponding excitation and emission wavelength imaged on the EVOS. B) Huh7.5 cells infected with YFV-17 expressing mScarlet and its corresponding excitation and emission wavelength imaged on the EVOS.

Luciferases: Bioluminescent Proteins

Bioluminescent proteins have been isolated from fireflies, deep sea shrimp, and other organisms and are a naturally occurring phenomenon (Figure 3) [42]. In these organisms, bioluminescent signal is produced when a substrate binds to a protein to generate light. In some cases, ATP is required to facilitate this reaction. In scientific

applications, luciferase is commonly used as a bioluminescent reporter enzyme that has helped to examine gene expression, monitor cellular process and many other applications. The benefit of luciferase reporters is their ability to be used in both *in vivo* and *in vitro* settings. Multi-wavelength imaging captures the emitted bioluminescence, allowing for a nuanced analysis and quantifiable measurement of bioluminescent signal [43,44]. Throughout their use, luciferase proteins have been modified to enhance signal strength, stability, and their effectiveness at reduced sizes. Unlike fluorescence-based techniques, bioluminescence does not require external excitation light, minimizing background noise and allowing for sensitive detection of low-level signals [45].

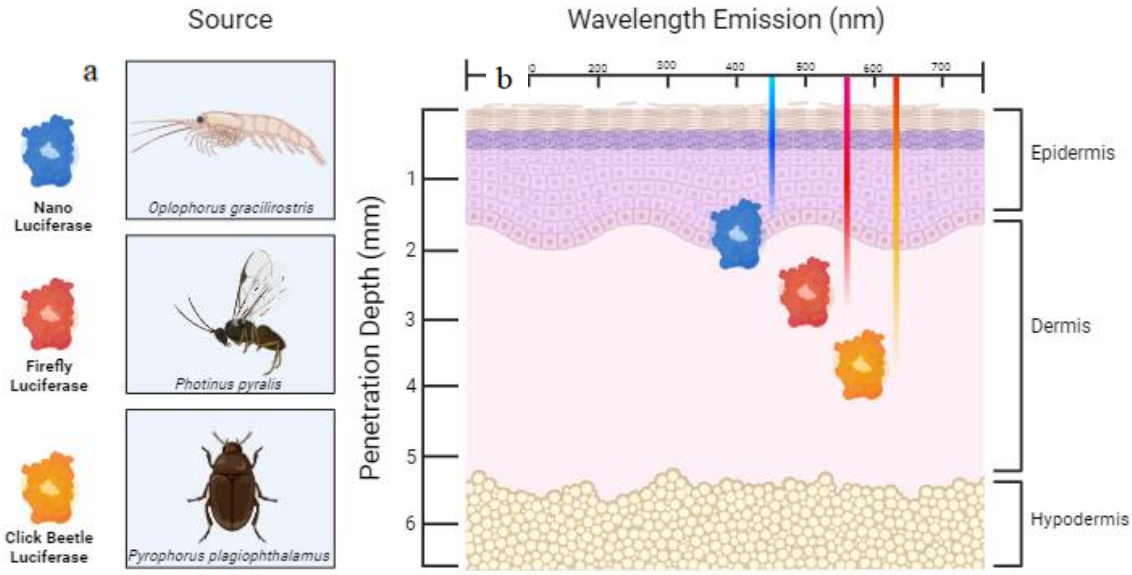

Figure 3: **Bioluminescent Reporter Proteins** A) Different types of reporter proteins and their sources from organisms present in nature B) Varying emission wavelengths of the three different reporter proteins and their corresponding penetration depths in human skin.

Nanoluc: Small but Bright

Originally derived from the deep-sea shrimp Oplophorus gracilirostris, Nanoluc (Nluc) stands out for its small size, rapid kinetics, and exceptional sensitivity. Compared to larger luciferases such as Firefly Luciferase (61kDA) and Renilla Luciferase (36kDA), Nluc's (19kDA) smaller size allows for enhanced cellular penetration and more efficient cloning into expression vectors [46]. Nluc utilizes furimazine (Fz) as a substrate, which binds to the enzyme and undergoes oxidation to generate an excited-state intermediate. This intermediate emits photons of light, producing a bright and stable luminescent signal with a peak wavelength of 460 nm. Since Nluc's discovery, there has been progress in substrate evolution, significantly amplifying the produced signal when compared to other luciferases [47]. This allows for a more sensitive readout of signal, requiring less protein to produce a comparable signal to the larger luciferase. Unlike fluorescent proteins, which require a continuous energy input for excitation, Nluc-mediated bioluminescence does not deplete cellular ATP levels, minimizing stress on adjacent tissues and cells [11,46]. Additionally, Nluc exhibits remarkable stability, retaining its luminescent activity even after fixation with formalin, expanding the utility of Nluc in a wide range of experimental settings [47].

Limitations of Reporter Viruses

The use of fluorescent and bioluminescent reporters in viral systems presents some challenges, particularly in balancing reporter size with viral genome constraints. Viruses, with their small genomes, tend to expel non-essential genomic material such as reporter proteins, to enhance their fitness [48]. This expulsion can significantly impact

viral replication kinetics or even result in the loss of the reporter gene during replication. For instance, while large luciferase reporters like firefly and click beetle luciferase may offer advantages such as higher emission wavelengths required for deeper tissue signal penetration, the virus they've been introduced to might expel the reporter after the only the a few replication cycles, rendering either the reporter obsolete or the virus non-functional because of mutations [49]. In addressing these challenges, Nluc has emerged as a promising reporter gene for studying viral infections [11].

Successfully implemented in various RNA viruses, including Hepatitis C virus (HCV) and Severe Acute Respiratory Syndrome Coronavirus 2 (SARS-CoV-2), Nluc demonstrates only moderate effects on infection dynamics [2]. However, its emission wavelength within the deep blue spectrum (350 to 495 nm), poses limitations for *in vivo* imaging. Blue light, being rapidly absorbed by tissues, can only penetrate a depth of approximately 0.3mm dermal tissue, resulting in weaker signals from an *in vivo* perspective [11, 44]. This limitation hinders the early detection of viral replication, as signals from low-level infections may be absorbed or might be too weak to be detected [50].

To overcome these limitations, adaptations have been made to improve signal intensities associated with Nluc [51]. Researchers at Promega have adapted both substrate and enzyme constructs to significantly enhance signal intensity compared to previous iterations of the reporter protein. However, this enhancement introduces another challenge: with increased signal intensity, the localization of signals at deeper tissue depths becomes more difficult. While the improved signal intensity is advantageous for

detecting viral infections, especially at early stages, the difficulty in localizing signals in deeper tissues poses practical challenges for *in vivo* imaging [52].

Bioluminescent Resonance Energy Transfer Reporter Systems

Bioluminescent Resonance Energy Transfer (BRET) leverages the transfer of energy between a bioluminescent donor protein, such as luciferase, and an acceptor fluorophore, enabling visualization of interactions at higher wavelengths and deeper tissue depths [53]. When a luciferase enzyme reacts with its substrate, it results in the emission of light. Bound to the luciferase donor is a fluorescent acceptor, such as a green fluorescent protein (GFP) or a red fluorescent protein (RFP), that emit fluorescence when excited by light of a specific wavelength (Figure 4). In the context of BRET signaling, energy is transferred when photons emitted by the luciferase enzyme are absorbed by the fluorescent protein, leading to energy transfer and fluorescent signaling [54].

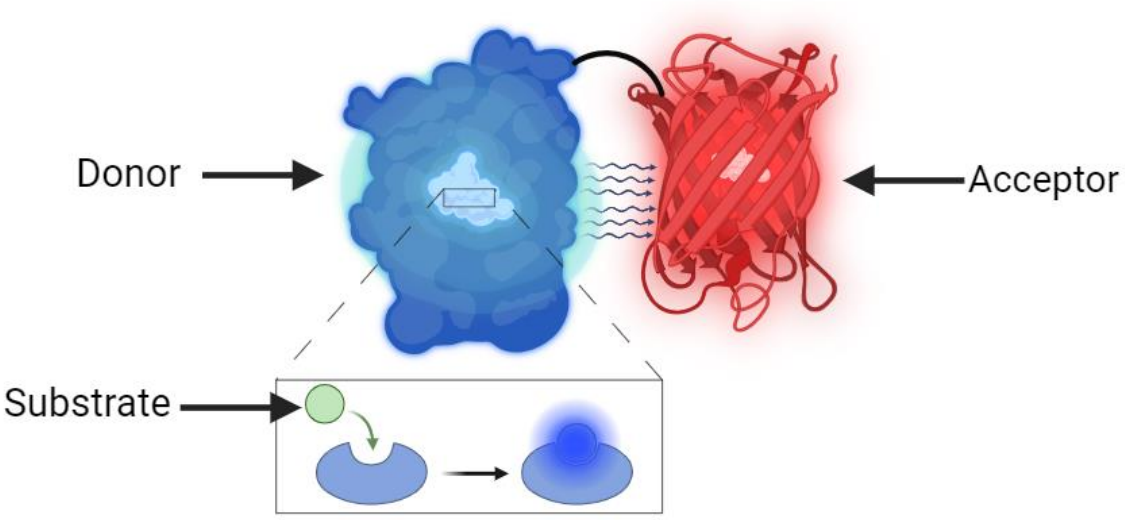

Figure 4: BRET Construct Depicting the Interaction Between Substrate, Donor Protein, and Acceptor Fluorophore

A mechanism involved in BRET signaling that allows for minimal spectral overlap is a long stokes shift (LSS). LSS refers to the difference between the excitation and emission wavelengths of a donor and acceptor proteins. In the case of reporter proteins that exhibit a long stokes shift, they can absorb light at a specific wavelength and emit photons at a significantly longer wavelength. Longer emission wavelengths are less prone to absorption by biological tissues, making them ideal for imaging through thick tissues and facilitating deeper tissue light penetrance [55].

Developing a BRET system that utilizes Nluc as a donor protein and an acceptor fluorescent protein that emits signal at a higher wavelength could address some of the limitations of Nluc, particularly the issue of Nluc having sub-optimal tissue penetrance for *in vivo* studies.

Circular Polymerase Extension Reaction System

Over the past decade, the circular polymerase extension reaction (CPER) system has been employed to rescue positive-strand RNA viruses and incorporate reporter genes into their genomes [9].

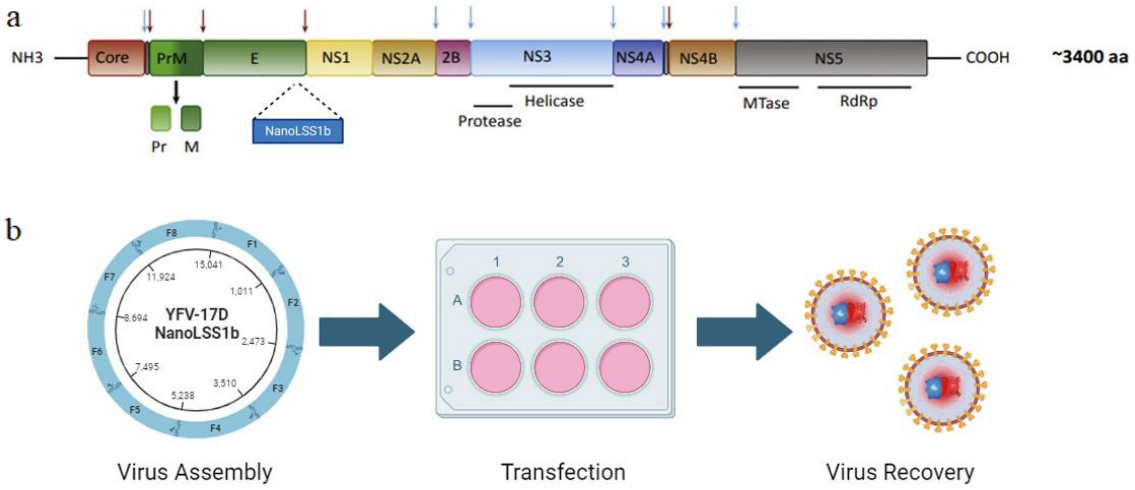

Figure 5: **Recombinant System to Incorporate Reporter Genes** A) Representation of YFV viral polyprotein with the novel reporter (NanoLSS1b) inserted between the E and NS1 proteins. B) Stages of the CPER reaction beginning by designing the virus fragments required for the full virus assembly, transfecting them in permissive cells followed by recovering virus particles expressing the reporter protein NanoLSS1b.

The general principle behind the CPER system (Figure 5) is to assemble full-length viral genomes without the need for virus specific reagents. Using DNA polymerase, overlapping fragments of the virus are annealed and extended to form the complete circular DNA molecule. The flexibility of CPER allows for allows for the modification of certain nucleotides of the viral genome or inclusion of various reporter proteins. When transfected into permissive cells, the host cell machinery transcribes the viral genome, producing viral particles with the desired modifications at a high titer. This tool can be used to generate YFV constructs expressing reporter viruses without disrupting the functionality of the virus [9].

Goal of the Study

Traditional bioluminescent reporters like Nluc face limitations in *in vivo* imaging due to suboptimal emission wavelengths and high signal intensities, which hinders signal localization. By combining Nluc with RFP into a single polyprotein, we were able to produce a novel reporter system (NanoLSS1) that utilizes a BRET system to address these challenges. This advancement allowed for enhanced signal intensity without compromising the localization of signals at deeper tissue depths. The goal of this study is to characterize this novel bioluminescent reporter system. We show that NanoLSS1 emits signal at a higher wavelength compared to Nluc, improving tissue penetration, and enabling multi-wavelength signal observations.

Future goals will involve the confirmation of NanoLSS1 increased signal intensity and penetration abilities *in vivo* upon 17D infection, enabling to gain novel insights into the propagation of YFV within the host. This tool will open avenues for an increased understanding of the viral and host determinants defining YFV virulence and attenuation, and for evaluating novel antiviral drugs against this virus.

METHODS

BSL-2 / BSL-3 Practices

Good laboratory practice and strict adherence to standard operating procedures were implemented when handling potentially harmful biological specimens.

All YFV-17D isolates were handled inside a Class II Biological Safety Cabinet (BSC) following BSL-2 practices. This included all tissue culture work, transfections, and plaque assays. Personal protective equipment (PPE) such as lab coats, gloves, and eye protection were always worn when handling biological specimens.

Since the IVIS was in the BSL-3 suite, all experiments that involved using the imager required following BSL-3 procedures, including dawning on the appropriate PPE, and following the appropriate enter and exit procedures. Personnel entering the BSL-3 suite must wear solid-front and back-closing Tyvek suits, double gloves, foot covers, arm sleeves and either be fitted for an N-95 respirator, or a HEPA filtered Powered Air Purifying Respirator (PAPR).

Tissue Culture

Huh 7.5 and 293T cells were cultured under standard conditions to ensure optimal growth and viability. Cells were maintained at 37°C in a humidified incubator with an atmosphere of 5% CO2. The culture medium used was Dulbecco's Modified Eagle Medium (DMEM) supplemented with 5% fetal bovine serum (FBS) and 1% penicillin-streptomycin. Cells were passaged at approximately 80-90% confluency to maintain healthy growth and to prevent over confluency [65].

Generation of NanoLSS1 Lentivirus

Human embryonic kidney 293T cells (HEK293T) were transfected with a calcium phosphate transfection to generate NanoLSS1a or NanoLSS1b lentivirus. To do this, 3x10^5 293T cells were plated in 6-well plate 24 hours prior to transfection. A mixture of 1µg of VSV g (plasmid 14888), 175ng of Gag Pol (plasmid add gene 14887), and 50 ng of plasmids encoding pcDNA3.1 (NanoLSS1). Media was changed 12-16 hours post-transfection; cells were incubated in a cell culture incubator at 37°C 5% CO2 for 48 hours. Supernatant containing lentivirus was collected at 48 hours post transfection, filtered with a 0.22 µm filter, and stored at -80°C [56,57].

Generation of NanoLSS1 Cell Lines

Human lung adenocarcinoma cells (A549) were transduced with NanoLSS1, NanoLSSS1a or 3xFT control lentivirus and incubated. This was done by plating 40,000 A549 cells in a 24-well plate for the day prior to transduction. Next day, media was removed, and 1 mL of lentivirus was added to cells and incubated 24 hours [57,58].

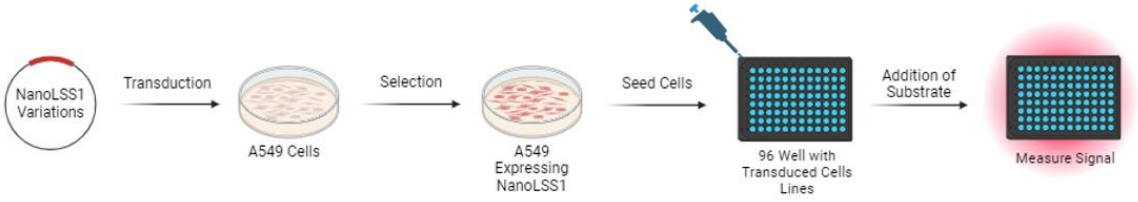

Figure 6: **Transduction Workflow** A549 cells were transduced to express the different reporter constructs to be later plated and imaged when supplemented with furimazine medium.

By transducing A549 cells with lentiviral particles carrying variations of the NanoLSS1 protein and the original Nluc protein, we generated four different cell lines expressing different versions of the reporter proteins and one cell lines expressing Nluc.

This approach allowed us to study the behavior and characteristics of the reporter proteins in a controlled setting, providing insights into their function and utility for future experimental applications.

IVIS Imaging

Images and measurements for Figures 10, 11, and 12 were acquired using the in vivo imaging systems (IVIS) (Perkin Elmer, MA). An open wavelength channel was used to detect all luminescent signal detected from the samples between 500 and 840 nm. Followed by this capture, the IVIS would detect and quantify luminescence through wavelength channels in increments of 20 nm from 500 to 840 nm.

Wavelength Tissue Depth Penetration

The various transduced cell lines were plated at equal densities on a black 96 well plate, with each variation seeded across two columns of the plate. The following day, furimazine was added, and the plate was imaged using the IVIS system. First, images were captured under an open wavelength channel to detect overall signal emission, followed by imaging through the 640 nm wavelength channel.

On the same 96 well plate, 2mm slices of ham (purchased from a grocery store) were placed across the top of plate and imaged periodically on the IVIS after each 2mm slice. Signal intensities of each column were recorded through the open wavelength channel. This was meant to compare signal intensities of each reporter construct to Nluc and to replicate tissue depth from an *in vitro* perspective. Images and calculations are displayed in Figures 11 and 12.

PrimeStar PCR Amplification

For the PCR reactions, each 50 µl reaction mixture contained 50-100 nM of whole YFV-17D plasmid, 10 µM of the forward primer, 10 µM of the reverse primer, 25 µl of PrimerSTAR Max DNA Polymerase, and nuclease-free water to reach a total volume of 50 µl. This setup was repeated eight times, each time using a different set of forward and reverse primers to amplify different fragments of the plasmid. The primers are listed in the figure below. Once the reaction mixtures were prepared, they were aliquoted into separate PCR tubes. The tubes were then placed in a thermal cycler and subjected to the following conditions: initial denaturation at 98°C for 10 seconds, followed by 35 cycles of 98°C for 10 seconds, 55°C for 2 seconds, and 72°C for 30 seconds. Finally, an extension was performed at 72°C for 120 seconds. The reactions were then held at 4°C until ready for further analysis [59].

Agarose Gel Preparation and Extraction

Agarose gel electrophoresis was performed to separate DNA fragments. To prepare the gel, 3.5 grams of agarose powder were dissolved in 35 ml of 1X TAE buffer by heating in a microwave for 45 seconds until fully dissolved. After cooling slightly, 2.45 µl of Cybersafe DNA stain was added and mixed thoroughly. The solution was then allowed to cool to approximately 50-60°C before being poured into a gel casting tray with a comb to create wells. The gel was left to solidify at room temperature for 20-30 minutes. Once solidified, the comb was removed, and the gel was placed in an electrophoresis apparatus submerged in 1X TAE buffer. PCR products mixed with gel loading dye were loaded into the wells along with a DNA ladder. The gel was run at 100-

120 volts for 30-60 minutes. After electrophoresis, DNA bands were visualized using a UV transilluminator, and desired bands were carefully excised with a scalpel.

For gel extraction, the excised gel slices were transferred to microcentrifuge tubes and weighed. Three volumes of gel-dissolving buffer were added, and the mixture was incubated at 50-60°C for 10-15 minutes until the gel was completely dissolved. The dissolved gel solution was applied to a spin column in a collection tube and centrifuged at 13,000 rpm for 1 minute to bind the DNA to the column membrane. The column was washed with 700 µl of wash buffer followed by centrifuging at 13,000 rpm for 1 minute and discarding the flow-through. The column was centrifuged for an additional 1 minute to remove residual wash buffer. DNA was eluted by adding 30-50 µl of elution buffer or nuclease-free water to the center of the column membrane, incubating for 1 minute at room temperature, and centrifuging at 13,000 rpm for 1 minute. The concentration and purity of the eluted DNA were measured, and the DNA was stored at -20°C until further use.

Primer Name	Primer Sequence	Region of YFV Amplified	Fragment Amplified
EC-001	gctcgtttagtgaaccgtagtaaatcctgtgtgctaattgaggt	5' UTR - PrM	F1 FWD
EC-002	gtaattccaatgcagtgagctgagtaggccggaccaacagc		F1 REV
EC-003	ttggtccggcctactcagctcactgcattggaat	E Protein	F2 FWD
EC-017	attaattgcacagccctggtccgccccaactcctagagacaaaaa		F2 REV

EC-018	tgtctctaggagttggggcggaccagggctgtgcaattaa	NeonGreen-DenV Linker	F3 FWD
EC-019	aagttgatggcgcatccttgatccgcttgaaccatgactccta		F3 REV
EC-020	gtcatggttcaagcggatcaaggatgcgccatcaact	NS1-NS2A	F4 FWD
EC-006	agtgcctcattcactgggatactccttcgcccaaatatg		F4 REV
EC-007	caacccgcatatttgggcgaaggagtatcccagtgaatgaggcac	NS2B-NS3	F5 FWD
EC-008	aactagcacttcagcagctcccctcctaccttcagcaaactta		F5 REV
EC-009	aatttattaagtttgctgaaggtaggaggggagctgctgaagtgctagtt	NS4A-NS4B	F6 FWD
EC-010	aaagtttttccattcgcgctccccggcgtccagttttcatcttccatagattgta		F6 REV
EC-011	tatggaagatgaaaactggacgccgggggagcgcgaatggaaaaacttt	NS5-3' UTR	F7 FWD
EC-014	aggtggagatgccatgccgacccttaagtggttttgtgtttgtcatccaaa		F7 REV
EC-015	atgacaaacacaaaaccacttaagggtcggcatggcatcctcca	Linker Protein	F8 FWD
EC-016	cacctcaattagcacacaggatttactacggttactaaacgagct		F8 REV

Table 1: Primers used to amplify YFV-17D expressing Neon Green.

TOPO Vector Cloning

The previously amplified and gel purified YFV-17D fragments are cloned into a pcDNA mammalian expression vector plasmid [60]. Stellar competent cells were employed to introduce the PCR fragments and the pcDNA vector. The competent cells, containing the cloned vector, were cultured at 37 ℃ and left overnight to achieve confluence. The transformation product was subsequently plated on agar for antibiotic selection, The transformed bacterial cells contain a plasmid expressing a Kanamycin resistance gene that when plated on Kanamycin infused agar, selects for bacterial isolates

that have successfully been cloned. Colonies were chosen from the plate and cultured in TB broth, followed by plasmid extraction using the MACHEREY-NAGAL Plasmid kit. The extracted plasmids underwent screening through restriction enzyme digestion and DNA sequencing [61].

Initiating the CPER Reaction

After amplifying and synthesizing all the cDNA fragments, 0.05 pmol of each fragment was calculated, and the eluted fragments were diluted to concentrations that could be aliquoted to a minimum volume of 1 µL. For the PCR reaction, the mixture (total volume: 50 µL) contained 10 µL of Primestar GXL polymerase, 4 µL of dNTPs, 10 µL of 5X buffer, 8 cDNA fragments, and nuclease-free water to adjust the total volume to 50 µL. The PCR protocol began with an initial denaturation at 98°C for 2 minutes, followed by 34 cycles of denaturation at 98°C for 10 seconds, annealing at 55°C for 15 seconds, and extension at 68°C for 15 minutes. A final extension was performed at 68°C for 15 minutes, and the reaction was then held at 25°C in the thermal cycler. The total reaction time was approximately 10 hours, allowing it to be left overnight if necessary. For a negative control, the reaction was replicated omitting one large fragment (F7).

Ligation of Circular Products

To seal the nicks between all the bound overlapping fragments, 1 µL of NAD+, 1 µL of Hifi Taq ligase is added to PCR reaction at room temperature. The reaction is placed in a thermal cycler and put at 50°C for 30 minutes, 60°C for 30 minutes and kept at 25°C. This is the final product to be used in the reverse transfection process [9].

Reverse Transfection

A confluent T75 flask of 293T cells was trypsinized by first removing the media using a vacuum suction pipette, then washing the cells with 5 mL of PBS distributed evenly using a "T" movement. The PBS was removed, and 2 mL of Trypsin was added to the flask, ensuring complete coverage of the surface. The flask was incubated at 37°C for 2-3 minutes until the cells detached. After the cells had fully detached, 8 mL of DMEM was added to the flask, and the mixture was pipetted up and down to create a single-cell suspension. One milliliter of this suspension was transferred back into the flask for future use, and the remaining suspension was used for plating. This is repeated for another flask of Huh7.5 cells.

To obtain a cell count in the suspension, 10 µL of trypan blue was mixed with 10 µL of the cell suspension to achieve a 1:1 dilution, which was then loaded into a hemocytometer. An automated cell counter was used to take eight images and calculate the average cell count per mL. 1*10^6 293T cells are resuspended in 3.5 ml of DMEM to be used for reverse transfection.

The CPER reaction is mixed with 500 µL of OptiMEM and 12 ul of Mirus TransIT-X2® Dynamic Delivery System in an Eppendorf tube. After incubating for 20 minutes, the transfection mixture is added into the 293T cell suspension which is later plated on to 2 wells of a 6 well plate. While the reaction is taking place, 2*10^6 Huh7.5 cells are seeded onto a T75 flask.

The next day, the media from both the flask and wells in replaced by DMEM supplemented with 2% FBS. The now transfected 293T cells are collected by flushing

directly with the overlaying media are then co-cultured with the Huh7.5 cells in the T75 flask. The difference in overall morphology between the two cell lines can be observed under a bright field microscope.

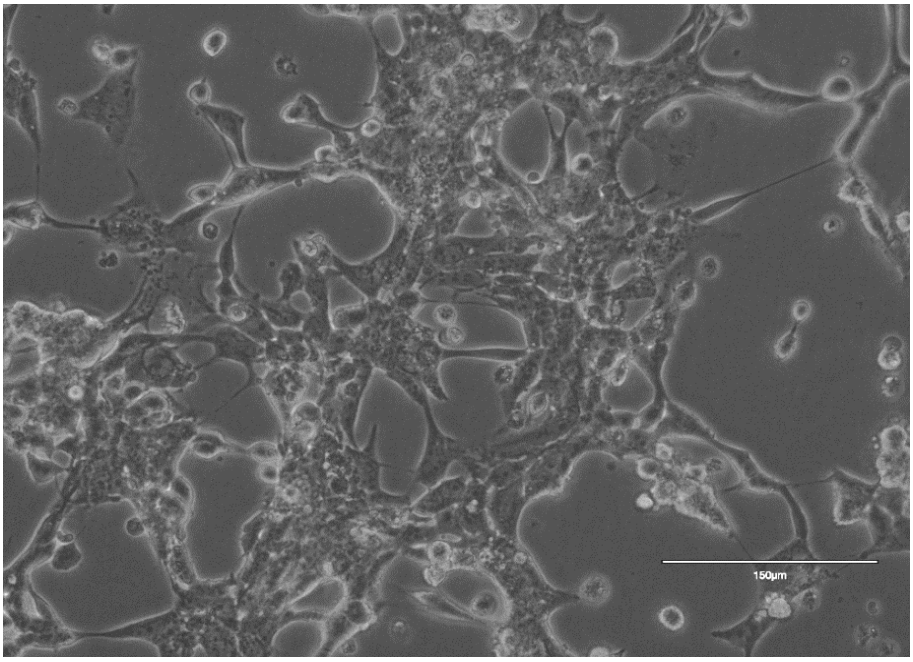

Figure 7: Co-cultured Huh7.5 and 293T cells on Day 1 of the CPER reaction.

Over the next two days, infected media is collected and replaced with fresh media. After two days, all cells will have dyed off and CPE can be seen across the flask. The pooled supernatant is spun at 300g to remove any cellular debris and passed through a 0.22um filter to be later used in a plaque assay to quantify the number of live infectious particles.

Making 2X DMEM

To make the overlay medium required for plaque assays, 13.4g of DMEM powder, 3.7g of NaHCO3, 10 ml of NA Pyruvate, 10 ml of Penicillin Streptomycin, 100

ml of FBS and enough DI water are added to a flask on a heat block to get the total volume to 500 ml.

Quantifying Viral Titers

To perform a plaque assay to quantify the viral titer of a Yellow Fever Virus 17D stock, Huh7.5 cells were plated on a 24-well plate. The cell suspension was diluted to 90,000 cells/mL, and each well of a 24-well plate was seeded with 1 mL of this suspension, resulting in 90,000 cells per well. The cells were incubated for 24 hours to allow for adhesion. To enhance cell adhesion, the wells were treated with poly-L-lysine prior to seeding the wells.

The viral stock obtained from the CPER reaction was prepared by performing 10-fold serial dilutions. 900 µL of plain DMEM was aliquoted in each of five Eppendorf tubes. 100 µL of the virus stock were added to the first tube and mixed thoroughly. From this first tube, 100 µL was transferred to the second tube, mixed, and this process was repeated until all five tubes contained serially diluted virus solutions. The media was removed from the wells of the 24-well plate, and 200 µL of each viral dilution was added to the wells, starting with the lowest concentration. The cells were incubated for 6 hours at 37°C. For the overlay, equal parts of 2X DMEM and 20% methyl cellulose were mixed.

After the 6-hour incubation, the viral inoculum was removed from each well, and 1 mL of the overlay solution was added to each well. The plates were incubated for 96 hours while being cautious as to not agitate the plate during incubation. After 96 hours, the overlay was carefully removed from the wells, which were then washed with 1 mL of

PBS. To fix the cell, 1 mL of 4% PFA was added to each well and incubated for at least 1 hour. In a fume hood, the PFA was removed, and the wells were stained with crystal violet solution for at least 1 hour. The crystal violet was suctioned off after staining and the plate was washed off with water and allowed to dry. Plaques were counted in wells containing 15-40 plaques for accurate quantification.

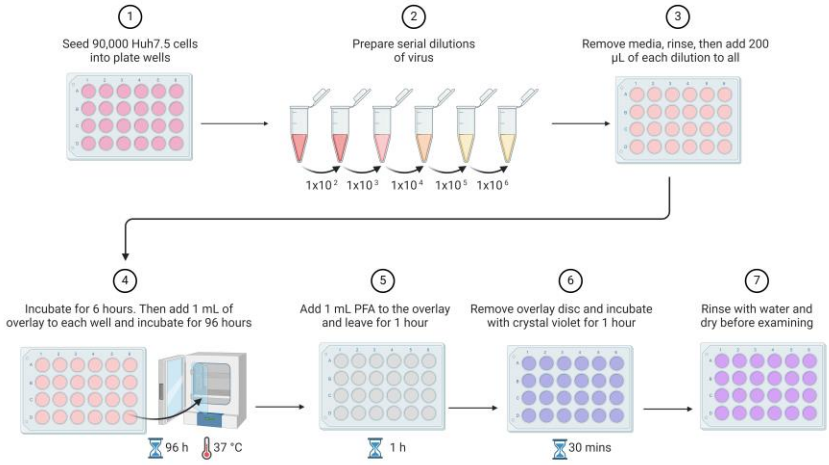

Figure 8: Plaque Assay Procedure Step by step procedure on how to perform a plaque assay.

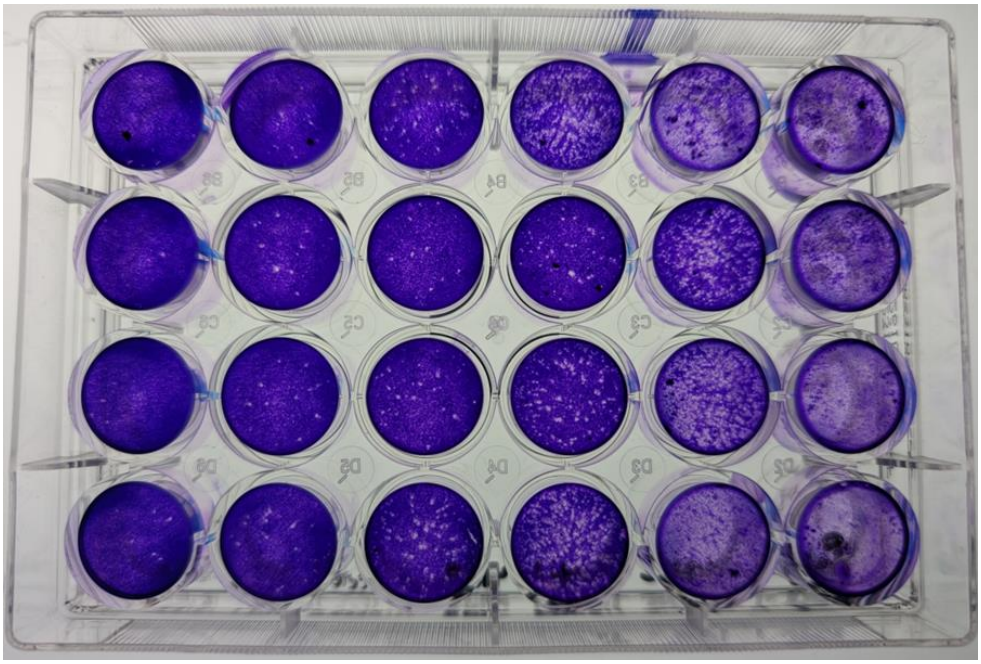

Figure 9: Stained Plaque Assay A 24 well stained plaque assay plate showing wells with a completely blown out monolayer of Huh7.5 cells and others with visible plaques. The first row quantified the viral titer of P0 of YFV-17D-NanoLSS1b. The second row quantified the viral titer of P1 of YFV-17D-NanoLSS1b. The third row quantified the viral titer of P0 of YFV-17D-Nluc. The fourth row quantified the viral titer of P1 of YFV-17D-Nluc.

Generating Fragments Containing NanoLSS1b and Nluc

To generate a fragment containing NanoLSS1b to be used in the CPER reaction, the Neon Green reporter was put in its place NanoLSS1b. Through restriction enzyme digestion, the plasmid containing the YFV-17D expressing the neon green protein was linearized.

1mg of plasmid, 1ng of AgeI restriction enzyme and enough nuclease free water was added to a tube get the reaction to reach 50 ul. After incubating at 37C for 1 hour, the reaction underwent gel electrophoresis and then gel purified.

The primers used to amplify the NanoLSS1b and Nluc fragments are mentioned in the table below.

Primer #	Sequence	Amplified Region
DL-1157	aatttcgggaccggtatggtcttcacactcgaaga	AgeI to Nluc
DL-1158	gaacgcattctggcgggcgccgcaacaaacttctct	Nluc to P2A
DL-1159	gtttgttgcggcgcccgccagaatgcgttcgcacagc	P2A to Nluc
DL-1160	gaacattttaccggtcggtccaggattctcttcgacat	DENV to P2A
DL-1103	taatttcgggaccggatggtctctaagggtgagg	AgeI FWD
DL-1104	cgaacattttaccggcggtccaggattctcttc	AgeI REV

Table 2: Primers needed to amplify NanoLSS1b and Nluc genes.

The fragments are amplified using Q5 polymerase in a 50ul volume. 10ul of Q5 reaction buffer, 1 ul of dNTPs, 2.5ul of forward primer, 2.5 ul of reverse primer, 10 ul of high GC enhancer, 0.5 ul of Q5 high fidelity polymerase and enough nuclease free water to get it to 50ul are aliquoted into a 200ul tube. The tubes were then placed in a thermal cycler and subjected to the following conditions: initial denaturation at 95°C for 2 minutes, followed by 5 cycles of 95°C for 15 seconds, 63°C for 15 seconds, and 72°C for 45 seconds followed by another 25 cycles of 95°C for 15 seconds and 72°C for 45 seconds to be finally kept at 4°C for later use. After the PCR cycle is complete, the resulting product was subjected to electrophoresis on a 1% agarose gel for size-based separation. The DNA fragments were then purified using the MACHEREY-NAGAL PCR cleanup kit [62,63].

PCR Gradient

Following the same conditions mentioned in Generating Fragments Containing NanoLSS1b and Nluc, a PCR gradient was set up to troubleshoot amplifying the F8 fragment required for the CPER reaction. Primers EC-15 and EC-16 from Table 1 were used were used to amplify a segment of the YFV-17D-NeonGreen backbone using Q5 Polymerase. Tubes were prepared in the same manner as the previous section and then placed in a thermal cycler and subjected to the following conditions: initial denaturation at 95°C for 2 minutes, followed by 5 cycles of 95°C for 15 seconds, followed by ranging annealing temperatures between 60°C and 70°C and for 15 seconds, and 72°C for 45 seconds followed by another 25 cycles of 95°C for 15 seconds and 72°C for 45 seconds to be finally kept at 4°C for later use. Based on the length and intensity of the band in the agarose gel, it was excised out following the Agarose Gel Extraction method.

Bacterial Transformations

Using the Takara 5X Infusion Snap Assembly, 10-200ng of the purified PCR fragments, 50-200ng of the linearized vector, 2 µl of 5X Infusion mix and enough nuclease free water to get the reaction to 10 µl are aliquoted into a 200 µl tube. The reaction is incubated for 15 minutes at 60°C then placed on ice.

JM109 competent cells were thawed on ice prior to adding 2 µl of the infusion mixture to 50 µl aliquots of the bacterial cells. The tube is placed on ice for 30 minutes, heat shocked at 42°C for 45 seconds, and then placed on ice for another 2 minutes. SOC medium is warmed up to 37°C before being added to the competent cells to bring the

final volume to 500 µl. This mixture is incubated for 1 hour at 37°C while shaking at 225 rpm.

The competent cells, containing the transformation mixture, were diluted at 1/10 ratio, and then subsequently plated on agar for antibiotic selection, utilizing Carbenicillin and Kanamycin.

After incubating overnight at 37°C, colonies were chosen from the plate and cultured in TB broth, followed by plasmid extraction using the MACHEREY-NAGAL Plasmid kit. The extracted plasmids underwent screening through restriction enzyme digestion and DNA sequencing [64].

Quantification of Bioluminescence Signals from Fixed Cells

The Varioskan™ LUX Multimode Microplate Reader (Thermo Fisher Scientific Inc., Waltham, MA, USA) was used to image fixed Huh7.5 cells infected with the YFV isolates expressing NanoLSS1b and Nluc. A 6 well plate seeded with 200,000 Huh7.5 cells was infected with the same dose of virus on each well (M.O.I. = 0.1). Cells were fixed with 4% PFA at 24, 48 and 72 hours. After the addition of Fz, luminescence was measured at 1000ms intervals through an open wavelength channel using the 6 well plate format.

RESULTS

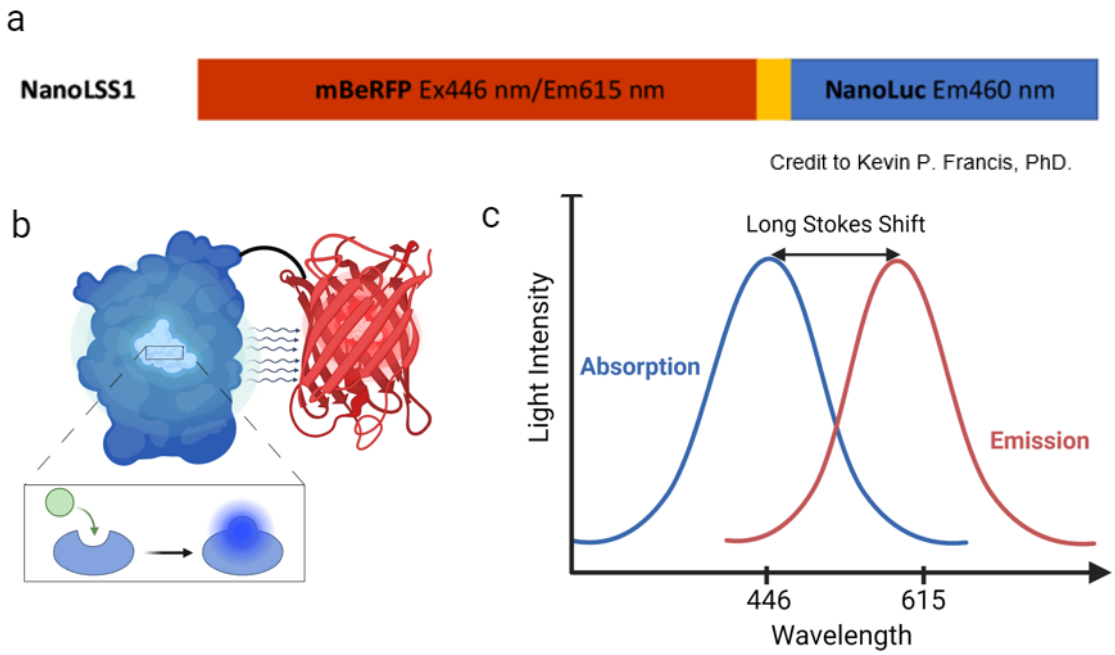

Figure 10: **NanoLSS1 Reporter Functionality** A) A breakdown of the fusion between mBeRFP and Nluc to produce NanoLSS1b and their corresponding excitation and emission wavelengths. B) Functional depiction of how the donor and acceptor proteins of NanoLSS1b act when reacting with furimazine C) Graph showing the absorptions and emission wavelengths of NanoLSS1b signified by a long stokes shift

Our collaborator, Kevin P. Francis, PhD, designed a NanoLSS1 reporter system by fusing a fluorescence reporter mBeRFP to Nluc (Figure 10A). mBeRFP has an excitation wavelength close to the emission wavelength of Nluc. When near an excited Nluc, mBeRFP emits signal at a higher wavelength, forming the basis for the long stokes shift reporter (Figure 10B-C). As seen in Figure 3, signal emitted at 615 nm can penetrate through much deeper tissue depth allowing for more robust and localized signal observations from *in vivo* studies.

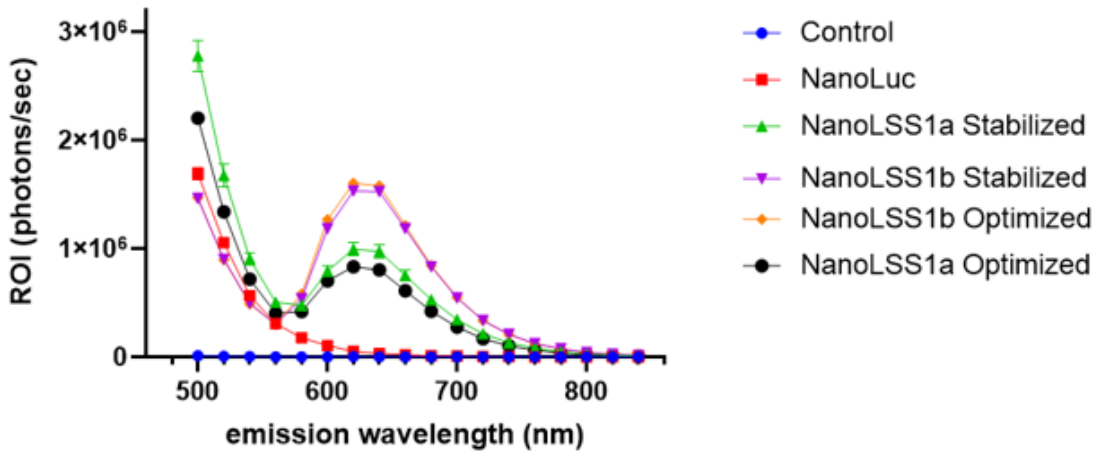

Figure 11: **BRET Wavelength Characterization** Different emission wavelengths of 6 transduced A549 cell lines in 20nm increments captured by the IVIS system.

We obtained multiple variations of NanoLSS1, which required a decision to narrow down the choice to one or two variations of the reporter to be used in future experiments. The different variations of NanoLSS1 (noted a and b) represent two distinct conformational changes the reporter system undergoes when the substrate is consumed and bioluminescent signal is produced. A stabilized version of NanoLSS1 has less variance in the conformational change, while a codon optimized version has been modified for a higher translation efficiency in mammalian cell lines.

The different constructs were transduced into A549 cells (see Wavelength Tissue Depth Penetration in Methods), seeded in a black well 96 well plate, and treated with Fz. An IVIS system was then used to compare the emission wavelength of the different constructs. Non-transfected A549 cells were used as a negative control. The lowest wavelength channel on the IVIS was 500nm so the emission peak at 460 nm of Nluc

could not be visualized. We were however able compare the BRET function of a and b variations of the NanoLSS1 reporter systems. All NanoLSS1 constructs displayed a robust emission peak at 615 nm compared to Nluc, as predicted (Figure 11). Construct variations a and b appear to drive the main emission differences at 615 nm across constructs. Optimization and stabilization did not impact emission peak. The a variation had a higher R.O.I at 500 nm compared to the b variations while the b variations had a higher R.O.I at 615 nm. The conformational change that NanoLSS1b underwent when reacting with Fz produced a higher R.O.I at a higher wavelength which is preferred for *in vivo* imaging to reduce the amount of signal absorbed by surrounding tissues.

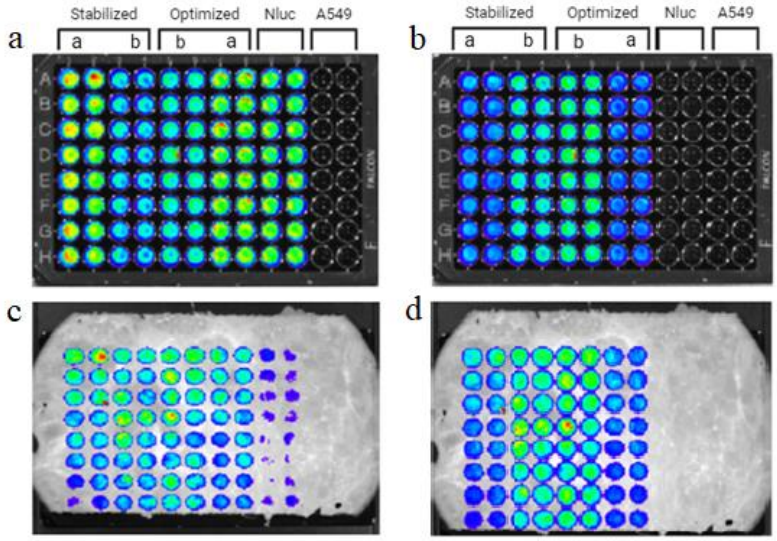

Figure 12: BRET Signaling Captured Using IVIS The same 96 Well plate seeded with A549 cells transduced with NanoLSS1a stabilitized and optimized, NanoLSS1b stabilized and optimized, Nluc and an non-transduced cell line supplemented by furimazine was imaged under an open different conditions using the IVIS. Cell lines were seeded in duplicate rows beside each other. A) An open wavelengh channel from 500 to 880nm. B) A 640-wavelength channel C) An open wavelengh channel from 500 to 880nm with the plate overlayed with ham D) A 640-wavelength channel with the plate overlayed with ham.

We validated our findings using a 96 well black well plate, to reduce any spillover of signal between the transduced cell lines (Figure 12A-B). We used both an open filter and a 640 nm channel, and image bioluminescent signals using the IVIS camera. Captured under an open wavelength channel of the IVIS (Figure 12A), all transduced cell lines emitted signal after Fz was added onto each well (Figure 12B). However, at 640 nm, only NanoLSS1 (all variations) signals were detected.

Interestingly, after a 2mm layer of ham was added on the plate, there was a stronger loss of signal for Nluc compared to NanoLSS1 variations under an open wavelength channel as shown in Figure 12C.

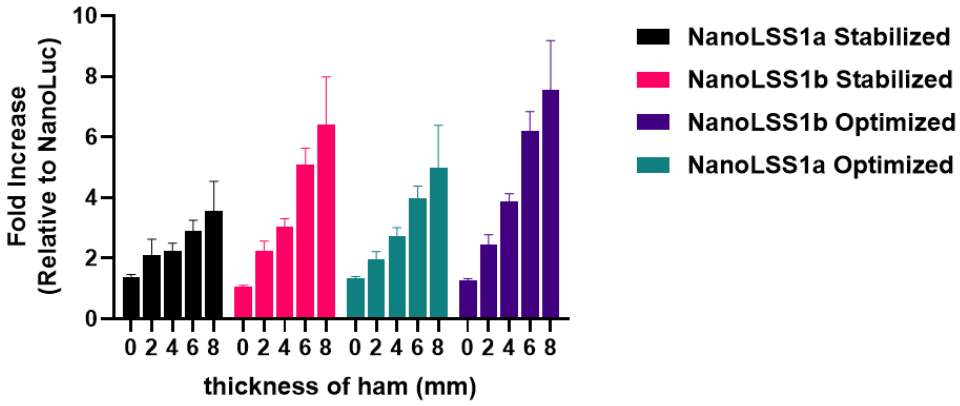

Figure 13: **Signal Fold Increase Relative to Nluc** Varying signal intensities captured on the open wavelength channel of the IVIS each captured after the addition of 2 mm of ham.

On the same black well plate from Figure 12, 2mm layers of ham were added periodically before each image capture on the IVIS through an open wavelength channel. Signal intensities of the different variations of NanoLSS1 were quantified and compared

relatively to Nluc. The optimized NanoLSS1b variation showed the highest fold increase of signal relative to Nluc (Figure 13) and the highest promise to be implemented for characterizing YFV-17D dissemination.

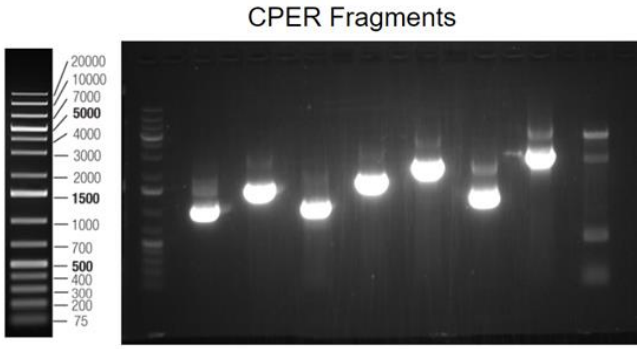

Figure 14: **PCR Amplified Fragments of YFV17D** The 7 different amplified fragments of YFV17D used in the CPER reaction imaged after gel electrophoresis. The final fragment was amplified separately using a PCR Gradient in the methods section.

We then moved forward in designing a YFV-17D recombinant virus expressing the optimized variation of NanoLSS1b. The whole YFV-17D Neon Green genome was used as a template to generate all 8 fragments required for the CPER reaction (Figure 14), and the fragment coding for Neon Green was swapped with one coding for NanoLSS1b. Primers from Table 1 were used following the PrimerStar amplification PCR methods. The DNA ladder confirmed that the lengths of the amplified fragments and signal intensity of the bands showed efficient binding of the primers and amplification of the product. Troubleshooting of amplifying fragment F8 (farthest to the right on Figure 14) needed to be implemented and is mentioned in the methods section PCR Gradient. YFV-17D-NanoLSS1 was then generated as described in the Methods section using the CPER system and reverse transfection.

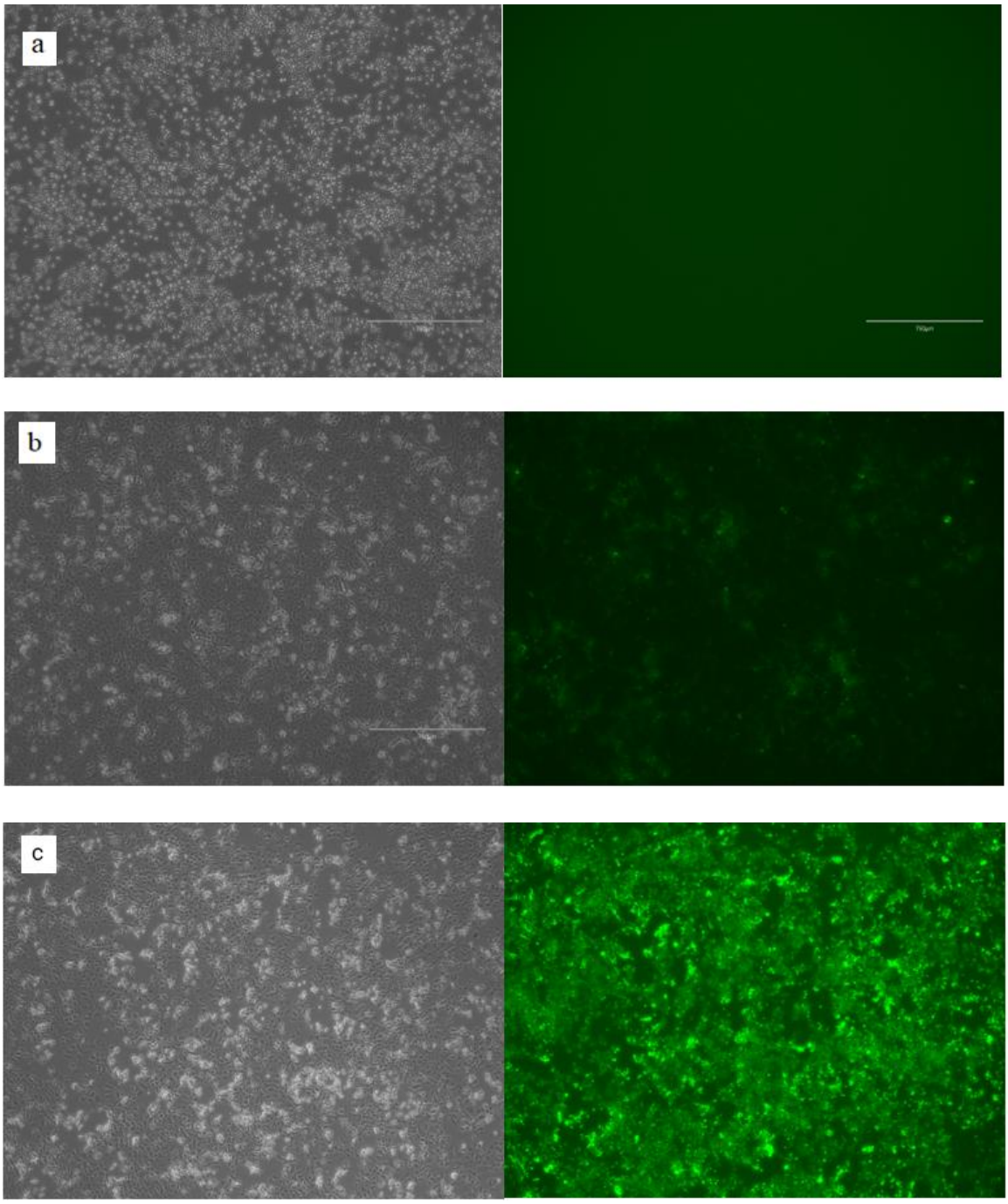

Figure 15: Spread of YFV-17D Neon Green made from CPER A) Huh7.5 cells infected with YFV-17D Neon Green 24 post reverse transfection under bright field and GFP lens imaged on the EVOS. B) Huh7.5 cells infected with YFV-17D Neon Green 48 post reverse transfection under bright field and GFP lens imaged on the EVOS. C) Huh7.5 cells infected with YFV-17D Neon Green 72 post reverse transfection under bright field and GFP lens imaged on the EVOS.

As a positive control of our CPER reaction, we also reconstituted a recombinant YFV-17D-NeonGreen. At 24 hours post reverse transfection, the cells showed no signs of cytopathic effects (CPE) under brightfield, and no NeonGreen fluorescence was observed (Figure 15). At 48 hours post transfection, some clusters of cells begin to change shape and detach from the well. Feint traces of NeonGreen signal was seen throughout monolayer of cells, showing that we were successful in generating a YFV-17D-NeonGreen. At 72 hours post transfection, all cells were noticeably expressing NeonGreen, further validating our success in reconstructing the recombinant 17D virus.

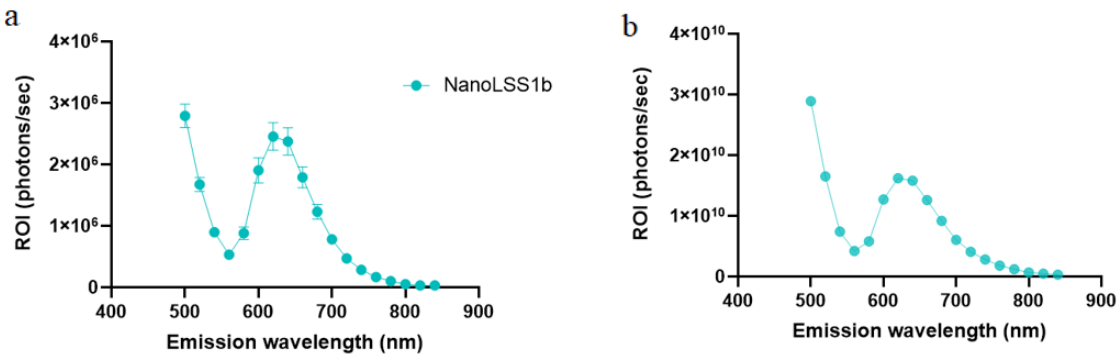

Figure 16: **BRET Functionality of NanoLSS1b** A) Exogenous expression of NanoLSS1b in A549 cells B) Huh7.5 cells infected with YFV-17D-NanoLSS1b.

Huh7.5 were infected with YFV-17D-NanoLSS1b from the initial CPER reaction (following co-culture with transfected HEK293t cells) and were fixed at 72h post-reverse transfection to quantify bioluminescent signals across emission wavelength.

Similarly, to NanoLSS1b-expressing cells, cells infected with YFV-17D-NanoLSS1b recapitulated BRET function (Figure 16), underscoring that our viral reporter could be implemented in *in-vivo* studies to track viral replication over time.

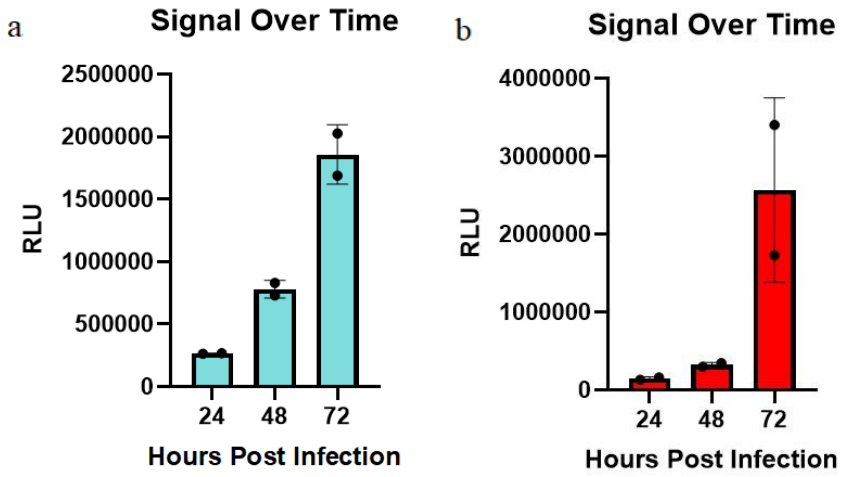

Figure 17: **Replication of YFV-17D- NanoLSS1b and -Nluc** A) Huh7.5 cells infected with YFV-17D-NanoLSS1b fixed with PFA at 24,48, and 72 hours imaged using the Varioskan LUX. B) Huh7.5 cells infected with YFV-17D-Nluc fixed with PFA at 24,48, and 72 hours imaged using the Varioskan LUX.

We then aimed to assess whether bioluminescence signals driven by YFV-17D-NanoLSS1 are resolutive enough to reflect viral spread dynamic across a cell layer, and infected Huh7.5 with a tittered stock of with YFV-17D-Nluc and YFV-17D-NanoLSS1b at a M.O.I. of 0.1. Indeed, NanoLSS1 bioluminescent signal incrementally increased over time in Huh7.5 following infection, and in a similar manner than cells infected with YFV-17D-Nluc (Figure 17). These findings underscore the ability of NanoLSS1-induced signals to recapitulate the dynamic of viral infection *in vitro*, highlighting the functionality of our reporter system for investigating multiple aspects of the 17D life

cycle *in vitro* and how it is regulated. Collectively, our reporter is now ready for *in vivo* characterization.

DISCUSSION

Summary

In this work, we report the characterization of a novel bioluminescent protein, NanoLSS1. We examined its functionality at different wavelengths using transfected cell lines expressing multiple variations of the reporter. NanoLSS1 showed a significant BRET function and emission peak at 615 nm, yielding to an increase in tissue depth penetration, addressing one of the limitations of Nluc. We also identified a specific variation of NanoLSS1, NanoLSS1b, to display the highest signal fold increase relative to Nluc and other NanoLSS1 variations at 615 nm.

Using the CPER system, we successfully incorporated NanoLSS1b and Nluc into YFV-17D. From this we validated that the BRET functionality of NanoLSS1b was retained in YFV-17D. Furthermore, NanoLSS1b-induced bioluminescence signals were resolutive enough to mirror incremental viral spread within an infected cell layer, highlighting the value of this reporter system to characterize YFV-17D infection. Collectively, our findings open avenues for the implementation of this reporter virus system to *in vivo* mouse infection to hopefully shed light on the infection dynamics of YFV-17D.

Future Experiments

Using YFV-17D-NanoLSS1b and -Nluc, the next step of this project will be to compare the infection dynamics of both viruses *in vivo* through a pilot study. One cohort of IFNAR K/O (Interferon alpha receptor Knockout) mice will be infected with YFV-17D-Nluc and another with YFV-17D-NanoLSS1b.

YFV-17D is unable to infect conventional, immunocompetent mice because infection is restricted by type I interferon [72]. In contrast, IFNAR K/O mice, which lack type I interferon receptors, are susceptible to YFV-17D infection, allowing researchers to study YFV-17D infection in a small animal model [73]. Since YFV-17D is a live attenuated virus, the experiment will be conducted in an ABSL-2 setting.

Every four days, mice will be injected intraperitoneally with a derivative of Fz and bioluminescence will be quantified spatially in each animal, for both NanoLSS1b and Nluc. This will allow us to compare the signal strength of both reporters through various tissue depths and define the increased ability of NanoLSS1b to uncover YFV-17D infection dynamics in many tissues. In parallel, additional mouse cohorts will be infected and tissues of interest will be collected at specific time point to validate that our two viruses display similar viral load in infected tissues; thereby excluding the possibility that differences in bioluminescence signals are driven by differential replication rate.

Future Directions of the Project

The increased tissue penetration of YFV-17D-NanoLSS1b opens up a wide range of investigations. First, we will be able to leverage the CPER system to incorporate NanoLSS1b into the more virulent Asibi strain of YFV. This will allow us to compare the infection dynamics of YFV-17D to its parent strain, unraveling key pathogenesis differences between virulent and attenuated form of YFV. Second, the incorporation of this reporter into virulent YFV strains and other flaviviruses will provide a pivotal tool to comprehensively characterize the antiviral activity of specific drugs, efficacy of novel vaccines or the roles of specific genes in regulating viral dissemination.

Limitations of the Study

One of the issues that arises when attempting to introduce foreign genes into a virus is that after several passages of the virus, the reporter gene is kicked out of the genome to enhance viral fitness. If the reporter negatively affects the fitness of the virus, then future lineages of the virus may no longer code for it [68].

A potential outcome from the *in vivo* infection studies would be that after several replication cycles, later passages of the virus might not express the reporter protein. The virus itself would still be replicating, but replication would not be associated with bioluminescent signals anymore. Another outcome would be that extensive replication rounds in tissues would cease to yield replicating viruses. One way to start addressing this potential limitation would be to serially passage the virus *in vitro* and monitor the stability of this reporter. During each passage, the viral titer of the supernatant will be calculated so that each novel round of infection is performed using the same multiplicity of infection (M.O.I.).

Signal strength would be the first variable to study reporter stability. The hope would be that NanoLSS1b expression and bioluminescent signal is preserved across passages and the signal intensity is relatively consistent. The other variable would be viral titer across passages [69]. Another limitation to this work is that there might be limited differences in bioluminescent signal resolution when comparing NanoLSS1b to Nluc *in vivo*. Although the *in vitro* comparison showed promise, the differences might not be as significant in vivo.

Conclusion

Understanding how specific viral mutations can affect viral pathogenesis and the course of disease is important to developing effective strategies against viral infections. Specific mutations can lead to changes in viral protein structure and/or function, which can enhance the virus's ability to replicate efficiently within the host, aid in immune evasion, and expand the range of tissues that the virus can infect. YFV is but an example of how a deviation of only a few nucleotides can lead to a much less virulent strain of a deadly virus.

Mutations can also lead to resistance to antiviral drugs, allowing for continued dissemination within the host and making it harder to control infection in immunocompromised patients.

Bioluminescent viral reporters can provide real-time, non-invasive, and quantitative data of the impact of viral mutations on viral dissemination, tissue tropism and pathogenesis. They can also represent instrumental tool to evaluate antiviral drugs in a cost-effective and rapid manner. Ultimately, the continuous development and refinement of bioluminescent reporter proteins represent an essential facet of our ability to effectively manage and mitigate viral diseases.

BIBLIOGRAPHY

1. Elena SF, Sanjuán R. Adaptive value of high mutation rates of RNA viruses: separating causes from consequences. Journal of Virology. 2005 Sep;79(18):11555-8. doi: 10.1128/JVI.79.18.11555-11558.2005. PMID: 16140732; PMCID: PMC1212614.
2. Hardin LT, Xiao N. miRNAs: The Key Regulator of COVID-19 Disease. International Journal of Cell Biology. 2022 Oct 29;2022:1645366. doi: 10.1155/2022/1645366. PMID: 36345541; PMCID: PMC9637033.
3. Frierson JG. The yellow fever vaccine: a history. Yale Journal of Biology and Medicine. 2010 Jun;83(2):77-85. PMID: 20589188; PMCID: PMC2892770.
4. Douam F, Ploss A. Yellow Fever Virus: Knowledge Gaps Impeding the Fight Against an Old Foe. Trends in Microbiology. 2018 Nov;26(11):913-928. doi: 10.1016/j.tim.2018.05.012. Epub 2018 Jun 19. PMID: 29933925; PMCID: PMC6340642.
5. Yeh HW, Ai HW. Development and Applications of Bioluminescent and Chemiluminescent Reporters and Biosensors. Annu Rev Anal Chem (Palo Alto Calif). 2019 Jun 12;12(1):129-150. doi: 10.1146/annurev-anchem-061318-115027. Epub 2019 Feb 20. PMID: 30786216; PMCID: PMC6565457.
6. Elegheert J, Behiels E, Bishop B, Scott S, Woolley RE, Griffiths SC, Byrne EFX, Chang VT, Stuart DI, Jones EY, Siebold C, Aricescu AR. Lentiviral transduction of mammalian cells for fast, scalable and high-level production of soluble and

membrane proteins. Nature Protocols. 2018 Dec;13(12):2991-3017. doi: 10.1038/s41596-018-0075-9. PMID: 30455477; PMCID: PMC6364805.

7. Yang J, Wang L, Yang F, Luo H, Xu L, Lu J, Zeng S, Zhang Z. mBeRFP, an improved large stokes shift red fluorescent protein. PLoS One. 2013 Jun 20;8(6):e64849. doi: 10.1371/journal.pone.0064849. PMID: 23840310; PMCID: PMC3688735.
8. Sureda-Vives M, Sarkisyan KS. Bioluminescence-Driven Optogenetics. Life (Basel). 2020 Nov 28;10(12):318. doi: 10.3390/life10120318. PMID: 33260589; PMCID: PMC7760859.
9. Torii S, Ono C, Suzuki R, Morioka Y, Anzai I, Fauzyah Y, Maeda Y, Kamitani W, Fukuhara T, Matsuura Y. Establishment of a reverse genetics system for SARS-CoV-2 using circular polymerase extension reaction. Cell Reports. 2021 Apr 20;35(3):109014. doi: 10.1016/j.celrep.2021.109014. Epub 2021 Apr 1. PMID: 33838744; PMCID: PMC8015404.
10. Krumpholz L, Clarke JF, Polak S, Wiśniowska B. An open-access data set of pig skin anatomy and physiology for modelling purposes. Database (Oxford). 2022 Oct 8;2022:baac091. doi: 10.1093/database/baac091. PMID: 36208224; PMCID: PMC9547536.
11. England CG, Ehlerding EB, Cai W. NanoLuc: A Small Luciferase Is Brightening Up the Field of Bioluminescence. Bioconjug Chem. 2016 May 18;27(5):1175-1187. doi: 10.1021/acs.bioconjchem.6b00112. Epub 2016 Apr 19. PMID: 27045664; PMCID: PMC4871753.

12. De Souza, W.M., Weaver, S.C. Effects of climate change and human activities on vector-borne diseases. Nature Reviews Microbiology (2024). https://doi.org/10.1038/s41579-024-01026-0

13. Frierson JG. The yellow fever vaccine: a history. Yale Journal of Biology and Medicine. 2010 Jun;83(2):77-85. PMID: 20589188; PMCID: PMC2892770.

14. Kopperman, Paul E. "The Philadelphia Yellow Fever Epidemic of 1793." *The Pennsylvania Magazine of History and Biography*, vol. 140, no. 1, 2016, pp. 73-98. JSTOR, www.jstor.org/stable/26070603

15. De Cock KM, Monath TP, Nasidi A, Tukei PM, Enriquez J, Lichfield P, Craven RB, Fabiyi A, Okafor BC, Ravaonjanahary C, et al. Epidemic yellow fever in eastern Nigeria, 1986. Lancet. 1988 Mar 19;1(8586):630-3. doi: 10.1016/s0140-6736(88)91425-0. PMID: 2894558.

16. Gardner CL, Ryman KD. Yellow fever: a reemerging threat. Clinics in Laboratory Medicine. 2010 Mar;30(1):237-60. doi: 10.1016/j.cll.2010.01.001. PMID: 20513550; PMCID: PMC4349381.

17. Lindsey NP, Horton J, Barrett ADT, Demanou M, Monath TP, Tomori O, Van Herp M, Zeller H, Fall IS, Cibrelus L, Erin Staples J. Yellow fever resurgence: An avoidable crisis? NPJ Vaccines. 2022 Nov 2;7(1):137. doi: 10.1038/s41541-022-00552-3. PMID: 36323723; PMCID: PMC9629880.

18. Kraemer MUG, Faria NR, Reiner RC Jr, Golding N, Nikolay B, Stasse S, Johansson MA, Salje H, Faye O, Wint GRW, Niedrig M, Shearer FM, Hill SC, Thompson RN, Bisanzio D, Taveira N, Nax HH, Pradelski BSR, Nsoesie EO,

Murphy NR, Bogoch II, Khan K, Brownstein JS, Tatem AJ, de Oliveira T, Smith DL, Sall AA, Pybus OG, Hay SI, Cauchemez S. Spread of yellow fever virus outbreak in Angola and the Democratic Republic of the Congo 2015-16: a modelling study. Lancet Infectious Diseases. 2017 Mar;17(3):330-338. doi: 10.1016/S1473-3099(16)30513-8. Epub 2016 Dec 23. Erratum in: Lancet Infect Dis. 2019 Apr;19(4):e109. doi: 10.1016/S1473-3099(19)30079-9. PMID: 28017559; PMCID: PMC5332542.

19. Quaresma JA, Barros VL, Pagliari C, Fernandes ER, Andrade HF Jr, Vasconcelos PF, Duarte MI. Hepatocyte lesions and cellular immune response in yellow fever infection. Transactions of The Royal Society of Tropical Medicine and Hygiene. 2007 Feb;101(2):161-8. doi: 10.1016/j.trstmh.2006.02.019. Epub 2006 Jul 26. PMID: 16872652.
20. De Brito T, Siqueira SA, Santos RT, Nassar ES, Coimbra TL, Alves VA. Human fatal yellow fever. Immunohistochemical detection of viral antigens in the liver, kidney and heart. Pathology Research and Practice. 1992 Feb;188(1-2):177-81. doi: 10.1016/S0344-0338(11)81176-3. PMID: 1594489.
21. Quaresma JA, Barros VL, Pagliari C, Fernandes ER, Guedes F, Takakura CF, Andrade HF Jr, Vasconcelos PF, Duarte MI. Revisiting the liver in human yellow fever: virus-induced apoptosis in hepatocytes associated with TGF-beta, TNF-alpha and NK cells activity. Virology. 2006 Feb 5;345(1):22-30. doi: 10.1016/j.virol.2005.09.058. Epub 2005 Nov 8. PMID: 16278000.

22. ter Meulen J, Sakho M, Koulemou K, Magassouba N, Bah A, Preiser W, Daffis S, Klewitz C, Bae HG, Niedrig M, Zeller H, Heinzel-Gutenbrunner M, Koivogui L, Kaufmann A. Activation of the cytokine network and unfavorable outcome in patients with yellow fever. International Journal of Clinical and Experimental Medicine. 2004 Nov 15;190(10):1821-7. doi: 10.1086/425016. Epub 2004 Oct 12. PMID: 15499539.

23. Quaresma JA, Barros VL, Pagliari C, Fernandes ER, Andrade HF Jr, Vasconcelos PF, Duarte MI. Hepatocyte lesions and cellular immune response in yellow fever infection. Transactions of the Royal Society of Tropical Medicine and Hygiene. 2007 Feb;101(2):161-8. doi: 10.1016/j.trstmh.2006.02.019. Epub 2006 Jul 26. PMID: 16872652.

24. Gianchecchi E, Cianchi V, Torelli A, Montomoli E. Yellow Fever: Origin, Epidemiology, Preventive Strategies and Future Prospects. Vaccines (Basel). 2022 Feb 27;10(3):372. doi: 10.3390/vaccines10030372. PMID: 35335004; PMCID: PMC8955180.

25. Gao Z, Zhang X, Zhang L, Wu S, Ma J, Wang F, Zhou Y, Dai X, Bullitt E, Du Y, Guo JT, Chang J. A yellow fever virus NS4B inhibitor not only suppresses viral replication, but also enhances the virus activation of RIG-I-like receptor-mediated innate immune response. PLoS Pathogens. 2022 Jan 21;18(1):e1010271. doi: 10.1371/journal.ppat.1010271. PMID: 35061864; PMCID: PMC8809586.

26. Hahn CS, Dalrymple JM, Strauss JH, Rice CM. Comparison of the virulent Asibi strain of yellow fever virus with the 17D vaccine strain derived from it.

Proceedings of the National Academy of Sciences of the United States of America. 1987 Apr;84(7):2019-23. doi: 10.1073/pnas.84.7.2019. PMID: 3470774; PMCID: PMC304575.

27. Lee E, Lobigs M. E protein domain III determinants of yellow fever virus 17D vaccine strain enhance binding to glycosaminoglycans, impede virus spread, and attenuate virulence. Journal of Virology. 2008 Jun;82(12):6024-33. doi: 10.1128/JVI.02509-07. Epub 2008 Apr 9. PMID: 18400851; PMCID: PMC2395160.
28. Fernandez-Garcia MD, Meertens L, Chazal M, Hafirassou ML, Dejarnac O, Zamborlini A, Despres P, Sauvonnet N, Arenzana-Seisdedos F, Jouvenet N, Amara A. Vaccine and Wild-Type Strains of Yellow Fever Virus Engage Distinct Entry Mechanisms and Differentially Stimulate Antiviral Immune Responses. mBio. 2016 Feb 9;7(1):e01956-15. doi: 10.1128/mBio.01956-15. PMID: 26861019; PMCID: PMC4752603.
29. Woodson SE, Freiberg AN, Holbrook MR. Differential cytokine responses from primary human Kupffer cells following infection with wild-type or vaccine strain yellow fever virus. Virology. 2011 Mar 30;412(1):188-95. doi: 10.1016/j.virol.2011.01.012. Epub 2011 Feb 1. PMID: 21277609.
30. Khaiboullina SF, Rizvanov AA, Holbrook MR, St Jeor S. Yellow fever virus strains Asibi and 17D-204 infect human umbilical cord endothelial cells and induce novel changes in gene expression. Virology. 2005 Nov 25;342(2):167-76. doi: 10.1016/j.virol.2005.07.035. Epub 2005 Sep 15. PMID: 16150475.

31. Palmer DR, Fernandez S, Bisbing J, Peachman KK, Rao M, Barvir D, Gunther V, Burgess T, Kohno Y, Padmanabhan R, Sun W. Restricted replication and lysosomal trafficking of yellow fever 17D vaccine virus in human dendritic cells. Journal of General Virology. 2007 Jan;88(Pt 1):148-156. doi: 10.1099/vir.0.82272-0. PMID: 17170447.
32. Gao Z, Zhang X, Zhang L, Wu S, Ma J, Wang F, Zhou Y, Dai X, Bullitt E, Du Y, Guo JT, Chang J. A yellow fever virus NS4B inhibitor not only suppresses viral replication, but also enhances the virus activation of RIG-I-like receptor-mediated innate immune response. PLoS Pathogens. 2022 Jan 21;18(1):e1010271. doi: 10.1371/journal.ppat.1010271. PMID: 35061864; PMCID: PMC8809586.
33. Monath TP, Vasconcelos PF. Yellow fever. Journal of Clinical Virology. 2015 Mar;64:160-73. doi: 10.1016/j.jcv.2014.08.030. Epub 2014 Oct 24. PMID: 25453327.
34. Belsher JL, Gay P, Brinton M, DellaValla J, Ridenour R, Lanciotti R, Perelygin A, Zaki S, Paddock C, Querec T, Zhu T, Pulendran B, Eidex RB, Hayes E. Fatal multiorgan failure due to yellow fever vaccine-associated viscerotropic disease. Vaccine. 2007 Dec 5;25(50):8480-5. doi: 10.1016/j.vaccine.2007.08.061. Epub 2007 Sep 18. PMID: 18023511; PMCID: PMC7115366.
35. https://wwwnc.cdc.gov/travel/yellowbook/2024/preparing/yellow-fever-vaccine-malaria-prevention-by-country

36. Harris E, Holden KL, Edgil D, Polacek C, Clyde K. Molecular biology of flaviviruses. Novartis Foundation Symposia. 2006;277:23-39; discussion 40, 71-3, 251-3. PMID: 17319152.

37. Germi R, Crance JM, Garin D, Guimet J, Lortat-Jacob H, Ruigrok RW, Zarski JP, Drouet E. Heparan sulfate-mediated binding of infectious dengue virus type 2 and yellow fever virus. Virology. 2002 Jan 5;292(1):162-8. doi: 10.1006/viro.2001.1232. PMID: 11878919.

38. Lee E, Lobigs M. E protein domain III determinants of yellow fever virus 17D vaccine strain enhance binding to glycosaminoglycans, impede virus spread, and attenuate virulence. Journal of Virology. 2008 Jun;82(12):6024-33. doi: 10.1128/JVI.02509-07. Epub 2008 Apr 9. PMID: 18400851; PMCID: PMC2395160.

39. Mukhopadhyay S, Kuhn RJ, Rossmann MG. A structural perspective of the flavivirus life cycle. Nature Reviews Microbiology. 2005 Jan;3(1):13-22. doi: 10.1038/nrmicro1067. PMID: 15608696.

40. Chiem K, Lorenzo MM, Rangel-Moreno J, Garcia-Hernandez ML, Park JG, Nogales A, Blasco R, Martínez-Sobrido L. Bi-Reporter Vaccinia Virus for Tracking Viral Infections *In Vitro* and *In Vivo*. Microbiology Spectrum. 2021 Dec 22;9(3):e0160121. doi: 10.1128/Spectrum.01601-21. Epub 2021 Nov 24. PMID: 34817228; PMCID: PMC8612144.

41. King CR, Mehle A. The later stages of viral infection: An undiscovered country of host dependency factors. PLoS Pathogens. 2020 Aug 25;16(8):e1008777. doi: 10.1371/journal.ppat.1008777. PMID: 32841303; PMCID: PMC7447017.

42. Vysotski, E.S. Bioluminescent and Fluorescent Proteins: Molecular Mechanisms and Modern Applications. International Journal of Molecular Sciences 2023, *24*, 281. https://doi.org/10.3390/ijms24010281

43. Chiem K, Lorenzo MM, Rangel-Moreno J, Garcia-Hernandez ML, Park JG, Nogales A, Blasco R, Martínez-Sobrido L. Bi-Reporter Vaccinia Virus for Tracking Viral Infections *In Vitro* and *In Vivo*. Microbiology Spectrum. 2021 Dec 22;9(3):e0160121. doi: 10.1128/Spectrum.01601-21. Epub 2021 Nov 24. PMID: 34817228; PMCID: PMC8612144.

44. Avci P, Gupta A, Sadasivam M, Vecchio D, Pam Z, Pam N, Hamblin MR. Low-level laser (light) therapy (LLLT) in skin: stimulating, healing, restoring. Semin Cutan Med Surg. 2013 Mar;32(1):41-52. PMID: 24049929; PMCID: PMC4126803.

45. Xu Y, Piston DW, Johnson CH. A bioluminescence resonance energy transfer (BRET) system: application to interacting circadian clock proteins. Proceedings of the National Academy of Sciences of the United States of America. 1999 Jan 5;96(1):151-6. doi: 10.1073/pnas.96.1.151. PMID: 9874787; PMCID: PMC15108.

46. Picard M, McEwen BS, Epel ES, Sandi C. An energetic view of stress: Focus on mitochondria. Frontiers in Physiology. 2018 Apr;49:72-85. doi:

10.1016/j.yfrne.2018.01.001. Epub 2018 Jan 12. PMID: 29339091; PMCID: PMC5964020.

47. Su Y, Walker JR, Hall MP, Klein MA, Wu X, Encell LP, Casey KM, Liu LX, Hong G, Lin MZ, Kirkland TA. An optimized bioluminescent substrate for non-invasive imaging in the brain. Nature Chemical Biology. 2023 Jun;19(6):731-739. doi: 10.1038/s41589-023-01265-x. Epub 2023 Feb 9. PMID: 36759751; PMCID: PMC10229426.
48. Subramanian T, Vijayalingam S, Chinnadurai G. Genetic identification of adenovirus type 5 genes that influence viral spread. Journal of Virology. 2006 Feb;80(4):2000-12. doi: 10.1128/JVI.80.4.2000-2012.2006. PMID: 16439556; PMCID: PMC1367173.
49. Campos LJ, Arokiaraj CM, Chuapoco MR, Chen X, Goeden N, Gradinaru V, Fox AS. Advances in AAV technology for delivering genetically encoded cargo to the nonhuman primate nervous system. Current Research in Neurobiology. 2023 Apr 7;4:100086. doi: 10.1016/j.crneur.2023.100086. PMID: 37397806; PMCID: PMC10313870.
50. Tamura T, Fukuhara T, Uchida T, Ono C, Mori H, Sato A, Fauzyah Y, Okamoto T, Kurosbu T, Setoh YX, Imamura M, Tautz N, Sakoda Y, Khromykh AA, Chaya ma K, Matsuura Y. 2018. Characterization of Recombinant Flaviviridae Viruses Possessing a Small Reporter Tag. J Virol 92:10.1128/jvi.01582-17.

51. Su, Y., Walker, J.R., Park, Y. et al. Novel NanoLuc substrates enable bright two-population bioluminescence imaging in animals. Nature Methods 17, 852–860 (2020). https://doi.org/10.1038/s41592-020-0889-6

52. Mary P. Hall, James Unch, Brock F. Binkowski, Michael P. Valley, Braeden L. Butler, Monika G. Wood, Paul Otto, Kristopher Zimmerman, Gediminas Vidugiris, Thomas Machleidt, Matthew B. Robers, Hélène A. Benink, Christopher T. Eggers, Michael R. Slater, Poncho L. Meisenheimer, Dieter H. Klaubert, Frank Fan, Lance P. Encell, and Keith V. Wood ACS Chemical Biology 2012 7 (11), 1848-1857DOI: 10.1021/cb3002478

53. Xia Z, Rao J. Biosensing and imaging based on bioluminescence resonance energy transfer. Frontiers in Physics. 2009 Feb;20(1):37-44. doi: 10.1016/j.copbio.2009.01.001. Epub 2009 Feb 11. PMID: 19216068; PMCID: PMC2680468.

54. Pfleger KD, Seeber RM, Eidne KA. Bioluminescence resonance energy transfer (BRET) for the real-time detection of protein-protein interactions. Nature Protocols. 2006;1(1):337-45. doi: 10.1038/nprot.2006.52. PMID: 17406254.

55. Shen Y, Chen Y, Wu J, Shaner NC, Campbell RE. Engineering of mCherry variants with long Stokes shift, red-shifted fluorescence, and low cytotoxicity. PLoS One. 2017 Feb 27;12(2):e0171257. doi: 10.1371/journal.pone.0171257. PMID: 28241009; PMCID: PMC5328254.

56. Leyva FJ, Anzinger JJ, McCoy JP Jr, Kruth HS. Evaluation of transduction efficiency in macrophage colony-stimulating factor differentiated human

macrophages using HIV-1 based lentiviral vectors. BMC Biotechnology. 2011 Jan 31;11:13. doi: 10.1186/1472-6750-11-13. PMID: 21281514; PMCID: PMC3045310.

57. Carpentier DC, Vevis K, Trabalza A, Georgiadis C, Ellison SM, Asfahani RI, Mazarakis ND. Enhanced pseudotyping efficiency of HIV-1 lentiviral vectors by a rabies/vesicular stomatitis virus chimeric envelope glycoprotein. Gene Therapy. 2012 Jul;19(7):761-74. doi: 10.1038/gt.2011.124. Epub 2011 Sep 8. PMID: 21900965.
58. Dull T, Zufferey R, Kelly M, Mandel RJ, Nguyen M, Trono D, Naldini L. A third-generation lentivirus vector with a conditional packaging system. Journal of Virology. 1998 Nov;72(11):8463-71. doi: 10.1128/JVI.72.11.8463-8471.1998. PMID: 9765382; PMCID: PMC110254.
59. Jia H, Guo Y, Zhao W, Wang K. Long-range PCR in next-generation sequencing: comparison of six enzymes and evaluation on the MiSeq sequencer. Scientific Reports. 2014 Jul 18;4:5737. doi: 10.1038/srep05737. PMID: 25034901; PMCID: PMC4102922.
60. Green MR, Sambrook J. Cloning Polymerase Chain Reaction (PCR) Products: TOPO TA Cloning. Cold Spring Harbor Protocols. 2021 Sep 1;2021(9). doi: 10.1101/pdb.prot101311. PMID: 34470863.
61. Mendoza EJ, Manguiat K, Wood H, Drebot M. Two Detailed Plaque Assay Protocols for the Quantification of Infectious SARS-CoV-2. Current Protocols in

Microbiology. 2020 Jun;57(1):ecpmc105. doi: 10.1002/cpmc.105. PMID: 32475066; PMCID: PMC7300432.

62. Pulendran, B. Learning immunology from the yellow fever vaccine: innate immunity to systems vaccinology. Nature Reviews Immunology 9, 741–747 (2009). https://doi.org/10.1038/nri2629
63. Monath TP, Vasconcelos PF. Yellow fever. Journal of Clinical Virology. 2015 Mar;64:160-73. doi: 10.1016/j.jcv.2014.08.030. Epub 2014 Oct 24. PMID: 25453327.
64. Hahn CS, Dalrymple JM, Strauss JH, Rice CM. Comparison of the virulent Asibi strain of yellow fever virus with the 17D vaccine strain derived from it. Proceedings of the National Academy of Sciences of the United States of America. 1987 Apr;84(7):2019-23. doi: 10.1073/pnas.84.7.2019. PMID: 3470774; PMCID: PMC304575.
65. Lee E, Lobigs M. E protein domain III determinants of yellow fever virus 17D vaccine strain enhance binding to glycosaminoglycans, impede virus spread, and attenuate virulence. Journal of Virology. 2008 Jun;82(12):6024-33. doi: 10.1128/JVI.02509-07. Epub 2008 Apr 9. PMID: 18400851; PMCID: PMC2395160.
66. Lindqvist R, Mundt F, Gilthorpe JD, Wölfel S, Gekara NO, Kröger A, Överby AK. Fast type I interferon response protects astrocytes from flavivirus infection and virus-induced cytopathic effects. Journal of Neuroinflammation. 2016 Oct

24;13(1):277. doi: 10.1186/s12974-016-0748-7. PMID: 27776548; PMCID: PMC5078952.

67. Nelson MD, Fitch DH. Overlap extension PCR: an efficient method for transgene construction. Methods in Molecular Biology. 2011;772:459-70. doi: 10.1007/978-1-61779-228-1_27. PMID: 22065455.

68. Li C, Chen X, Hu J, Jiang D, Cai D, Li Y. A Recombinant Genotype I Japanese Encephalitis Virus Expressing a *Gaussia* Luciferase Gene for Antiviral Drug Screening Assay and Neutralizing Antibodies Detection. International Journal of Molecular Sciences. 2022 Dec 8;23(24):15548. doi: 10.3390/ijms232415548. PMID: 36555192; PMCID: PMC9778660.

69. Kapałczyńska M, Kolenda T, Przybyła W, Zajączkowska M, Teresiak A, Filas V, Ibbs M, Bliźniak R, Łuczewski Ł, Lamperska K. 2D and 3D cell cultures - a comparison of different types of cancer cell cultures. Archives of Medical Science. 2018 Jun;14(4):910-919. doi: 10.5114/aoms.2016.63743. Epub 2016 Nov 18. PMID: 30002710; PMCID: PMC6040128.

70. Fernandez-Garcia MD, Meertens L, Chazal M, Hafirassou ML, Dejarnac O, Zamborlini A, Despres P, Sauvonnet N, Arenzana-Seisdedos F, Jouvenet N, Amara A. Vaccine and Wild-Type Strains of Yellow Fever Virus Engage Distinct Entry Mechanisms and Differentially Stimulate Antiviral Immune Responses. mBio. 2016 Feb 9;7(1):e01956-15. doi: 10.1128/mBio.01956-15. PMID: 26861019; PMCID: PMC4752603.

71. Woodson SE, Freiberg AN, Holbrook MR. Differential cytokine responses from primary human Kupffer cells following infection with wild-type or vaccine strain yellow fever virus. Virology. 2011 Mar 30;412(1):188-95. doi: 10.1016/j.virol.2011.01.012. Epub 2011 Feb 1. PMID: 21277609.

72. Meier KC, Gardner CL, Khoretonenko MV, Klimstra WB, Ryman KD. A mouse model for studying viscerotropic disease caused by yellow fever virus infection. PLoS Pathogens. 2009 Oct;5(10):e1000614. doi: 10.1371/journal.ppat.1000614. Epub 2009 Oct 9. PMID: 19816561; PMCID: PMC2749449.

73. Li XF, Li XD, Deng CL, Dong HL, Zhang QY, Ye Q, Ye HQ, Huang XY, Deng YQ, Zhang B, Qin CF. Visualization of a neurotropic flavivirus infection in mouse reveals unique viscerotropism controlled by host type I interferon signaling. Theranostics. 2017 Feb 12;7(4):912-925. doi: 10.7150/thno.16615. PMID: 28382163; PMCID: PMC5381253.

CURRICULUM VITAE